RESEARCH ARTICLE

The initiation and maintenance of CHH methylation and its effects on gene expression are unique in maize

Beibei Liu[1], Diya Yang[1], Dafang Wang[2], Chun Liang[1], Jianping Wang[3], Damon Lisch[4], Meixia Zhao[5, *]

[1] Department of Biology, Miami University, Oxford, OH 45056

[2] Biology Department, Hofstra University, Hempstead, NY 11549

[3] Agronomy Department, University of Florida, Gainesville, FL 32610

[4] Department of Botany and Plant Pathology, Purdue University, West Lafayette, IN 47907

[5] Department of Microbiology and Cell Science, University of Florida, Gainesville, FL 32611

[*]Address for correspondence: Meixia Zhao (meixiazhao@ufl.edu; tel 352-273-3715)

Running Title: CHH methylation in maize

Key words: *trans*-chromosomal interactions, DNA methylation, initiation and maintenance, differentially methylated regions

Abstract

Trans-chromosomal interactions resulting in changes in DNA methylation during hybridization have been observed in several plant species. However, very little is known about the causes or consequences of these interactions, many of which result in changes in methylation of transposable elements. Here, we compared DNA methylomes of F1 hybrids that are mutant for two small RNA biogenesis genes, *Mop1* (*mediator of paramutation1*) and *Lbl1* (*leafbladeless1*) with that of their parents, wild type siblings, and backcrossed progeny in maize. Our data show that hybridization triggers global changes in both *trans*-chromosomal methylation (TCM) and *trans*-chromosomal demethylation (TCdM). Despite changes in CHH methylation in F1 hybrids, no significant changes in the quantity or distribution of small RNAs were observed. The methylation at the CHH TCM differentially methylated regions (DMRs) was largely removed in the *mop1* mutant, although the effects of this mutant vary depending on the location of the CHH sites. Interestingly, an increase in CHH at TCM DMRs was associated with enhanced expression of a subset of highly expressed genes and suppressed expression of a small number of lowly expressed genes. Examination of the methylation levels in backcrossed plants demonstrates that the newly triggered methylation can be maintained to the subsequent generation, but that TCdM is maintained more stable than is TCM. Surprisingly, although increase CHH methylation in F1 plants did require *Mop1*, heritability of TCM or TCdMs did not require a functional copy of this gene, suggesting that initiation of these heritable changes in epigenetic state are not dependent on RdDM.

Introduction

DNA methylation is a heritable epigenetic mark involved in many important biological processes, such as genome stability, genomic imprinting, paramutation, development, and environmental stress responses (Matzke et al. 2015; Lewsey et al. 2016; Zhang et al. 2016; Erdmann and Picard 2020). In plants, DNA methylation commonly occurs in three cytosine contexts, the symmetric CG and CHG (where H = A, C, or T) contexts, and the asymmetric CHH context (Law and Jacobsen 2010; Matzke and Mosher 2014; Li et al. 2015b). In Arabidopsis, *de novo* methylation at all of these three cytosine contexts is catalyzed by domains rearranged methyltransferase 2 (DRM2) through the canonical RNA-directed DNA methylation (RdDM) pathway. In the canonical RdDM, single-stranded RNA is transcribed by RNA polymerase IV (Pol IV) and copied into double-stranded RNA by RNA-directed RNA polymerase 2 (RDR2). The dsRNA is then processed by Dicer-like 3 (DCL3) into 24-nucleotide (nt) small interfering RNAs (siRNAs), which can recruit histone modifiers and DNA methyltransferases back to the original DNA sequences to trigger methylation (Matzke and Mosher 2014; Matzke et al. 2015; Erdmann and Picard 2020). In maize, the targeted loci of canonical RdDM are primarily transposable elements (TEs) or other repeats near genes, where the chromatin is more accessible, rather than the deeply heterochromatic regions farther from genes (Gent et al. 2014; Li et al. 2015a). In addition to the canonical RdDM triggered by 24-nt siRNAs, some 21-22 nt siRNAs that are produced from Pol II-RDR6 (RNA polymerase II-RNA-directed RNA polymerase 6) derived transcripts and that typically function in posttranscriptional gene silencing (PTGS) can also direct RdDM, termed as non-canonical RdDM or RDR6 RdDM (Wu et al. 2012; Nuthikattu et al. 2013; Cuerda-Gil and Slotkin 2016). RDR6 RdDM acts on many long and autonomous TEs when they are transcriptionally active and plays a critical role in initiation and establishment of TE silencing (Nuthikattu et al. 2013; Panda et al. 2016). In plants, *de novo* methylation triggered by RdDM is maintained by different pathways depending on the location of the target sequences (Law and Jacobsen 2010). CG and CHG methylation are maintained during following DNA replication by methyltransferase 1 (MET1) and chromomethylase 3 (CMT3), respectively (Matzke and Mosher 2014; Matzke et al. 2015). CHH methylation is maintained through persistent *de novo* methylation by DRM2 through the RdDM pathway, which requires small RNAs and relatively open chromatin, or by chromomethylase 2 (CMT2) in conjunction with H3 lysine 9 dimethylation (H3K9me2) in deep heterochromatin, which does not (Stroud et al. 2014).

This complex system of chromatin modification ensures that epigenetic silencing is reliably transmitted from generation to generation. However, there are situations in which that stability can be perturbed. Hybrids are an example of this because hybridization brings together two divergent genomes and epigenomes in the same nucleus. The interaction between these divergent genomes can result in both instability and transfers of epigenetic information between genomes. It has been demonstrated that *trans*-chromosomal interactions of DNA methylation between parental alleles in F1 hybrids occur in many plant species, including Arabidopsis (Greaves et al. 2012; Shen et al. 2012; Greaves et al. 2015; Greaves et al. 2016; Zhang et al. 2016), rice (He et al. 2010; Chodavarapu et al. 2012; Ma et al. 2021), maize (Barber et al. 2012; He et al. 2013; Li et al. 2014), pigeonpea (Junaid et al. 2018), and soybean (Schmitz et al. 2013). In Arabidopsis F1 hybrids, significant changes in F1 methylomes involve *trans*-chromosomal methylation (TCM) and *trans*-chromosomal demethylation (TCdM), in which the methylation level of one parental allele is altered to resemble that of the other parental allele (Greaves et al. 2012; Greaves et al. 2016; Zhang et al. 2016; Junaid et al. 2018). Small RNAs, particularly 24-nt siRNAs, are associated with the methylation changes at the regions of the genome where methylation levels differ between the two parents (He et al. 2010; Groszmann et al. 2011; Chodavarapu et al. 2012; Shivaprasad et al. 2012; Greaves et al. 2016; Zhang et al. 2016). Small RNA sequencing in Arabidopsis, maize, wheat and rice has revealed a general decrease in 24-nt siRNAs in the hybrids at regions where parental siRNA abundance is different (He et al. 2010; Groszmann et al. 2011; Kenan-Eichler et al. 2011; Barber et al. 2012; Chodavarapu et al. 2012). In maize, the downregulation of 24-nt siRNAs following hybridization is observed in developing ears, but not in seedling shoot apex (Barber et al. 2012), suggesting either the tissue type or developmental stage is important for the changes in small RNAs observed in hybrids. It has been hypothesized that siRNAs produced from the methylated parental allele can trigger *de novo* methylation of the other parental allele when the two alleles are brought together in F1 hybrids (Greaves et al. 2012; Greaves et al. 2015). In Arabidopsis F1 hybrids, siRNAs from one allele are found to be sufficient to trigger methylation without triggering siRNA biogenesis from the other allele in F1 plants at TCM differentially methylated regions (DMRs) (Zhang et al. 2016), a process that is reminiscent of paramutation at many loci in maize (Arteaga-Vazquez and Chandler 2010; Hollick 2017).

The inheritance of both TCM and TCdM in subsequent generations can be meiotically stable across many generations but varies at different loci in Arabidopsis (Schmitz et al. 2011; Greaves et al. 2014; Greaves et al. 2016). In maize and soybean, parental methylation differences are inherited by recombinant inbred lines over multiple generations. However, these changes can be unstable, and are likely guided by small RNAs (Regulski et al. 2013; Schmitz et al. 2013). A recent study in maize identified thousands of TCM and TCdM loci in F1 hybrids. However only about 3% of these changes were transmitted through six generations of backcrossing and three generations of selfing (Cao et al. 2022), suggesting that the methylation status of any given locus is largely determined by local sequences. Most current research has focused on the initiation and maintenance of overall levels of DNA methylation, but the causes and consequences of DNA methylation depend on its context. In large genomes such as maize, regions distant from genes are typically maintained in a deeply heterochromatic state and are the CG and CHG sequence contexts. Methylation in gene bodies is largely in the CG context and is associated with high or variable levels of gene expression (Takuno and Gaut 2012; Muyle et al. 2022). In contrast, CHH methylation, which almost entirely dependent on RdDM in maize, occurs almost exclusively in regions immediately adjacent to genes, resulting in so-called “mCHH islands” (Gent et al. 2013; Li et al. 2015a). The result of this variation is a dramatically skewed distribution of methylated cytosines. In the maize reference genome, there are a total of 972,798,068 cytosines, out of which, 18.7% and 16.4% are CG and CHG cytosines, and 64.9% of which are CHH cytosines. Unlike CG and CHG methylation, which is ubiquitous, CHH methylation is extremely low, only 2.4% genome-wide, and is largely restricted to mCHH islands. This may be due to lack of CMT2 in maize, the major chromomethylase that functions in the maintenance of CHH methylation in heterochromatin in other plants. In maize, these CHH islands are thought be the boundaries between deeply silenced heterochromatin and more active euchromatin to promote and reinforce silencing of the TEs located near genes (Gent et al. 2013; Li et al. 2015a).

To understand the initiation and maintenance of CHH methylation and its effects on gene expression, we performed high-throughput sequencing of DNA methylomes, small RNA and mRNA of F1 hybrids that were mutant for two genes, *Mop1* (*mediator of paramutation1*) and *Lbl1* (*leafbladeless1*), and their parents and wild type siblings. *Mop1* is a sequence ortholog of *RDR2* in Arabidopsis, which is a major component of the canonical RdDM (Alleman et al. 2006). In the *mop1* mutant, 24 siRNAs are dramatically reduced (Nobuta et al. 2008; Gent et al. 2014),

which results in a near completely removal of CHH methylation near genes (Li et al. 2015a; Zhao et al. 2021), confirming a significant role for MOP1 in *de novo* CHH methylation in maize. LBL1 is a homolog of SGS3 (SUPPRESSOR OF GENE SILENCING3) in Arabidopsis, which works together with RDR6 to produce 21-22-nt *trans*-acting siRNAs, which are a key component of PTGS and non-canonical RdDM (Cuerda-Gil and Slotkin 2016).

Our results show that CHH methylation is increased globally in hybrids, but those increases are unequally distributed, resulting in new and distinctive patterns of methylation. While only the low-parent (the parent with the lower methylation level) allele gains methylation in CG and CHG TCM DMRs, both the high-parent (the parent with the higher methylation level) and low-parent alleles of CHH TCM DMRs gain methylation in F1 hybrids. Importantly, the increase in methylation in the low-parent alleles is not associated with the generation of allele specific small RNAs, suggesting that small RNAs from one allele is sufficient to trigger methylation in the other allele, but is not sufficient to trigger Pol IV transcription of the target allele. Interestingly, these CHH TCM DMRs are associated with the enhanced expression of a subset highly expressed genes and suppressed expression of a subset of lowly expressed genes. We refer to the former as “positive mCHH islands”, and the latter as “negative mCHH islands”, which are enriched for H3 lysine 27 trimethylation (H3K27me3) and depleted of H3 lysine 4 trimethylation (H3K4me3). Global reduction of methylation levels in CHH TCM DMRs was observed in the backcrossed (BC1) generation relative to the F1s, suggesting that maintenance of CHH methylation in this generation requires RdDM.

Results

CHH methylation level is globally increased in hybrids

To understand the initiation of DNA methylation, we crossed *mop1* heterozygous plants in the Mo17 and B73 backgrounds to each other (Mo17;*mop1-1/*+ × B73;*mop1-1/*+) to generate F1 hybrid *mop1* mutants (Mo17/B73;*mop1-1/mop1-1*, designated as *mop1*F1) and their hybrid homozygous wild type siblings (Mo17/B73;+/+, designated as WTF1) (Fig. 1A). We next performed whole genome bisulfite sequencing (WGBS) of the two parental genotypes (Mo17 and B73) and the two F1 hybrids (WTF1 and *mop1*F1) (Supplemental Table S1). The overall methylation levels of B73 (25.1%) and Mo17 (25%) were similar. We observed a substantial increase in overall methylation levels in WTF1 hybrids (30%) compared to the two parents

(25%), as has been noted previously in both Arabidopsis and maize (Supplemental Fig. S1 and Supplemental Table S2) (Zhang et al. 2016; Cao et al. 2022). The increased methylation was primarily driven by the increased CHH methylation, while CG and CHG were not dramatically changed (Fig. 1B and Supplemental Fig. S1,2). Interestingly, although the *mop1* mutation reduces CHH methylation (Zhao et al. 2021), overall levels of CHH methylation in *mop1*F1 was still higher than the two wild type parents (Fig. 1B and Supplemental Fig. S2), suggesting that the effect of hybridization in triggering methylation is stronger than that of *mop1* in reducing methylation globally.

Previous research had shown that *mop1* mutants primarily affect mCHH islands near active genes (Gent et al. 2014; Li et al. 2015a). Therefore, we plotted DNA methylation levels of CG, CHG and CHH within gene bodies, 3 kb upstream of TSSs (transcription start sites) and 3 kb downstream of TTSs (transcription termination sites). In genes, we observed similar patterns with respect to the methylation levels of CG and CHG between parents and F1 hybrids. In contrast, the methylation levels of CHH cytosines in both upstream and downstream of genes were dramatically increased in WTF1 plants, and dramatically reduced in the *mop1*F1 mutants relative to the two parents (Fig. 1C). We next determined CG, CHG and CHH methylation levels within TE bodies and their flanking regions. The distal edge of TEs relative to genes generally had higher levels of CG and CHG methylation than their proximal edge, as did the region immediately adjacent to the TEs. CHH methylation was increased in WTF1 hybrids across TE bodies and flanking regions, particularly the two edges of TEs. Interestingly, CHH methylation level at the proximal edge and the adjacent flanking regions of TEs in *mop1*F1 was lower than that in the two parents. In contrast, the CHH methylation level at the distal edge of TEs and the adjacent flanking regions in *mop1*F1 was only marginally reduced relative to WTF1, and was still higher than that in the parents (Fig. 1D). In the body of TEs, the increase in CHH methylation triggered by hybridization was unchanged in *mop1* mutants. Together, these data suggest that MOP1 is particularly important for CHH methylation of the portion of TEs that are near genes, along with the region between the TE and the gene. Outside of those regions, it would appear that MOP1 is not required for the increased CHH methylation. The net effect is a strong effect of *mop1* on the new mutation in CHH islands, but a much reduced effect on overall changes in DNA methylation seen in the F1.

Levels of CHH methylation of both high-parent and low-parent (parents with the higher and lower methylation levels) alleles are increased at TCM DMRs in the F1 hybrids

Changes in methylation in F1 hybrids occurs largely at regions that are already differentially methylated between parents (Zhang et al. 2016). We first identified DMRs between the two parents, Mo17 and B73, in our data set. Here we referred to these DMRs as parental DMRs, which can be Mo17 or B73 hyper DMRs, indicating that either Mo17 or B73 has a significantly higher level of DNA methylation (Fig. 2A). In total, we identified 7,107 CG, 9,045 CHG, and 13,307 CHH DMRs between the two parents (Fig. 2B and Supplemental Table S3). CHH DMRs were typically shorter than CG and CHG DMRs (Supplemental Fig. S3 and Supplemental Table S3). The B73 genome had more CG and CHG hyper DMRs, and the Mo17 genome had more CHH hyper DMRs, which is consistent with the observation that B73 had higher overall CG and CHG methylation and Mo17 had higher overall CHH methylation at these DMRs (Fig. 2B,C). We also found that CG and CHG DMRs were more overlapped with each other than each was with CHH DMRs (Fig. 2D), consistent with previous observations that CHH methylation is often found in mCHH islands immediately up and downstream of genes (Gent et al. 2013; Li et al. 2015a). Out of the 13,307 CHH DMRs, 52% were located within or near genes, particularly 2 kb upstream and downstream of genes (43%), which was significantly higher than the values for CG (27%) and CHG (18%) in these regions ($P < 0.0001$, χ^2 test) (Fig. 2E). Given that TEs are the primary targets of DNA methylation and maize genes are frequently adjacent to TEs (Li et al. 2015a; Erdmann and Picard 2020), we compared the different classes of TEs overlapping DMRs within the 2 kb flanking regions of genes. Not surprisingly, given their distribution within genomes, we found that terminal inverted repeat (TIR) DNA transposons were more enriched in CHH DMRs than they were in CG and CHG DMRs within 2kb of genes (Fig. 2E,F).

Next, we examined the methylation levels of these parental DMRs in the F1 hybrids. Following previously published studies, we compared the methylation levels of WTF1 to the mid-parent value (MPV, average of the two parents) and classified changes as being a consequence of TCM (*trans*-chromosomal methylation), TCdM (*trans*-chromosomal demethylation), or NC (no change) (Fig. 3A) (Zhang et al. 2016). A majority of parental DMRs (~75%) did not significantly change their methylation levels in the WTF1 hybrids, and most of these unchanged DMRs were in TEs and unclassified regions (Fig. 3A and Supplemental Fig. S4). However, when single nucleotide polymorphisms (SNPs) were used to distinguish

methylation in each of the two parental genomes, many of these NC DMRs in WTF1 were revealed to have lost methylation at the high-parent allele and gained methylation at the low-parent allele, which resulted in no significant changes in overall methylation levels between the hybrids and parents, suggesting that methylation interaction still occurs in these NC DMRs (Supplemental Fig. S5). Out of the 25% of the DMRs that were significantly changed, 18.7% were TCM, and 6.8% were TCdM (Fig. 3A). We then examined allele specific methylation levels of these regions using SNPs between B73 and Mo17. At TCM DMRs, WTF1 had higher methylation levels at all of the three cytosine contexts (Fig. 3B). The increased methylation at CG and CHG in these wild type F1 plants was primarily due to the increased methylation in the parental allele that had the lower level of methylation. In contrast, CHH methylation levels of both the high- and low-parent alleles were substantially increased in WTF1 at these TCM DMRs. Methylation was reduced in *mop1*F1 in all sequence contexts, especially CHH methylation, which was near completely removed in the mutant (Fig. 3B). The decreased methylation of TCdM in these *mop1* F1 plants was mainly due to decreased methylation of the high-parent allele (Fig. 3C).

Methylation of CHH TCM DMRs is dramatically reduced in the *mop1* mutant

To shed light on the effects of the *mop1* mutation on these parental DMRs, we examined their methylation levels in *mop1*F1 plants. Only 99 (8.6%) of 1,147 CG and 144 (11.2%) of 1,284 CHG TCM DMRs significantly changed their methylation levels in *mop1*F1 mutants. In contrast, methylation levels of 90.7% (1,031 out of 1,137) CHH TCM DMRs were significantly changed in *mop1*F1 (Fig. 4A). Consistent with our global analysis, the CHH DMRs that were significantly changed in *mop1* were primarily located in the 2 kb flanking regions of genes (Supplemental Fig. S6). As expected, methylation of all the three sequence contexts at these TCM DMRs were largely reduced in *mop1*F1 mutants, particularly in the CHH context, in which the methylation level in *mop1*F1 plants was even lower than the low parent (Fig. 4B). This suggests that in these regions, but not the genome as a whole, the additional methylation in F1 wild type plants is lost altogether. Not surprising, given that the methylation of TCdM DMRs was already very low, we did not observe significant changes in methylation at TCdM DMRs in the *mop1*F1 mutants (Fig. 4C).

Previous research has demonstrated that loss of methylation in mCHH islands results in additional loss of CG and CHG methylation (Li et al. 2015a). We found that out of the 118 CG

DMRs that were significantly changed in *mop1*F1 mutants relative to their wild type siblings, 37 (31.4%) were also CHG DMRs, but only 3 (2.5%) were CHH DMRs. Similarly, only 32 (20.9%) and 9 (5.9%) of the CHG DMRs that were changed in *mop1* were CG and CHH DMRs, respectively. Out of the 1,048 *mop1*-affected CHH DMRs, 72 (6.7%) and 181 (17.3%) were CG and CHG DMRs (Supplemental Table S4). A similar pattern was observed for the *mop1*-affected CHG DMRs, in which we detected changes in CG but no changes in CHH methylation. For *mop1*-affected CHH DMRs, we saw no change in CG but a substantial change in CHG (Fig. 4D). Together these data suggest that *mop1* mutation primarily prevents the methylation of CHH TCM DMRs, and that a loss of CHH methylation in *mop1* can result in additional loss of CHG, but not CG methylation.

Small RNAs from one allele are sufficient to trigger methylation of the other allele in F1 hybrids

Because small RNAs are the trigger for *de novo* DNA methylation (Matzke and Mosher 2014; Matzke et al. 2015), we next asked whether the difference in methylation during hybridization is caused by differences in small RNAs. We proposed two hypotheses with respect to siRNAs at the CHH TCM DMRs. As shown in Fig. 5A, in the first hypothesis, small RNAs are produced from one allele and trigger the methylation of both alleles in F1 hybrids. In the alternative hypothesis, both alleles in F1 plants generate small RNAs even though one of the derived parents (Parent 2 in Fig. 5A) does not produce small RNAs. To distinguish between these hypotheses, we performed small RNA sequencing from the same plants that were used for DNA methylation analysis (Supplemental Table S1). As was expected, 24-nt siRNAs were the most abundant siRNAs in all the sequenced samples. Overall, no significant changes in small RNAs were observed between the WTF1 hybrids and parents (Fig. 5B), despite the dramatic increase we observed in CHH methylation in the hybrids (Fig. 1B). The *mop1* mutation largely reduced 24-nt siRNAs, particularly in the mCHH island regions near TSSs and TTSs (Fig. 5B and Supplemental Fig. S7). Next, we compared 24-nt siRNAs generated from the high parent and low parent. We detected 24-nt uniquely mapped siRNAs in 795 CG (11.2% of the total), 700 CHG (7.7%), and 5,070 CHH (38.1%) parental DMRs. Consistent with their role in methylation, on average, the high parent harbored significantly more 24-nt siRNAs than the low parent (Supplemental Fig. S8). This is also true for TCM, TCdM, and NC DMRs when analyzed

separately (Supplemental Fig. S9), suggesting that small RNAs are the major trigger driving methylation differences at these DMRs between the two parents.

To test whether the increase in methylation in WTF1 plants was due to an increase in 24-nt small RNAs, we compared the abundance of 24-nt siRNAs between WTF1 and the MPV. siRNA levels were significantly lower in CG and CHG TCdM DMRs in hybrids than the MPVs, consistent with their decreased methylation levels in WTF1 (Supplemental Fig. S9). In contrast, although TCM DMRs gained methylation following hybridization, no significant increases in the abundance of siRNAs were detected in F1 hybrids (Fig. 5C and Supplemental Fig. S9). We then analyzed allele-specific expression of siRNAs in F1 hybrids. Because only uniquely mapped reads with SNPs can be used to access the allele specific expression of siRNAs and because the length (24-nt) of siRNAs is very short, we were only able to obtain data from 76 CHH TCM DMRs that had enough information to compare allele-specific expression. Among these 76 CHH TCM DMRs, 25 had siRNAs only in the high parent. Of these, 19 (76%) had siRNAs only produced from the high-parent allele in WTF1. There was no significant difference between the ratio of 24-nt siRNAs of the high-parent allele to the low-parent allele in F1 hybrids and that of the high parent to the low parent in the parents (Fig. 5D). These data suggest that the increased methylation at TCM DMRs is not caused by an increase in siRNAs from the newly methylated allele, which favors the hypothesis that small RNAs produced from one allele trigger methylation of the other allele in *trans*, but that the newly methylated allele is not a source of small RNAs.

RdDM triggered by small RNAs depends on the similarity of the small RNAs and their targets. Thus, the sequence variation between the two alleles may affect small RNA targeting and ultimately methylation. To test this, we compared the SNPs between TCM and TCdM. As shown in Fig. 5E, no significant differences in SNP enrichment were observed when comparing TCM and TCdM at CG and CHG DMRs. In contrast, CHH TCdM DMRs had a significantly more SNPs than did CHH TCM DMRs, suggesting that more genetic variation at CHH TCdM DMRs hinders targeting of one allele by small RNAs from the other allele.

CHH methylation of sequences flanking genes is associated with both suppressed and enhanced expression of neighboring genes

Given the variation we observed in the parental lines B73 and Mo17 (Fig. 2), we compared the activity of genes involved in the RdDM pathway in these genotypes. We compared the expression values of 51 genes in the RdDM pathway between B73 and Mo17. We detected eight

differentially expressed genes (DEGs), all of which showed significantly higher expression in the Mo17 genome (Supplemental Fig. S10 and Supplemental Table S5), which may contribute to the greater abundance of CHH methylation in the Mo17 genome (Fig. 2B,C). In addition, all of these differentially expressed RdDM pathway genes also had higher expression in the F1 hybrids than the MPV (Supplemental Fig. S10 and Supplemental Table S6), suggesting that the RdDM pathway is more active in hybrids.

DNA methylation is generally associated with repression of transcription, particularly when the methylation is in the promoter regions of genes (Zilberman et al. 2007; Hollister and Gaut 2009; He et al. 2011). However, recent studies have revealed that mCHH islands mark the transition from heterochromatin to euchromatin in maize and are often present at highly expressed genes (Li et al. 2015a). To understand the effects of changes in CHH methylation on gene expression, we investigated the correlation between the subset of CHH islands that gain methylation in F1 hybrids (TCM DMRs) with expression of genes that flank them. We proposed two different models for the effects of CHH methylation on gene expression, as shown in Fig. 6A and Supplemental Fig. S11A. For the Mo17 CHH TCM DMRs, whose methylation is transferred from Mo17 to B73, if methylation suppresses gene expression, because the Mo17 parent has higher methylation, we would expect it to have a lower level of expression. After hybridization, if the B73 allele gains methylation, it would be expected to produce less transcript. If this is the case, we would expect to see the ratio of gene expression of Mo17 to B73 in the F1 hybrids to increase relative to the ratio of expression of these alleles in the parents (Fig. 6A, left panel). In contrast, if CHH methylation promotes gene expression, we would predict a decrease in the ratio of gene expression of Mo17 to B73 in F1 hybrids (Fig. 6A, right panel). We focused on 442 Mo17 hyper DMRs with available allele-specific methylation in F1, 172 of which had available allele-specific expression data, and then looked for genes whose allele-specific expression changed significantly in F1 relative to the parents. Of the genes flanking the 172 Mo17 hyper DMRs, 126 (73%) associated with those DMRs showed no significant change in relative expression. For 16 genes, the ratio of Mo17 to B73 expression was increased, and for 31 genes, the ratio was decreased in the F1 hybrids (Fig. 6B), suggesting that CHH methylation can be associated with both suppressed and enhanced gene expression. We next compared the expression of these 16 and 31 genes between parents B73 and Mo17. As proposed in the model (Fig. 6A), the expression of the 16 genes that seemed to be suppressed by CHH methylation was

significantly lower in Mo17 than in B73. In contrast, the expression of the 31 genes whose expression seemed to be enhanced by CHH methylation was higher in Mo17 than in B73 parents (Supplemental Fig. S11B), although higher CHH methylation in the promoter of Mo17 parent was detected in both scenarios.

Next, we asked why variation in expression of genes is associated with variation in histone modifications. The 16 DMRs that were associated with suppressed gene expression were significantly enriched for H3K27me3 and depleted of H3K4me3 in B73 (Fig. 6C and Supplemental Fig. S11C) (Ricci et al. 2019). The 31 genes that seemed to be enhanced by CHH methylation were typically longer, more highly expressed, and with higher gene body methylation than the 16 suppressed genes in Mo17 (Fig. 6D and Supplemental Fig. S11D). Because the *mop1* mutation results in reduced methylation in mCHH islands near genes (Li et al. 2015a; Zhao et al. 2021), we wanted to determine whether removal of methylation of the 16 and 31 DMRs in the *mop1* mutant changed the expression of their flanking genes. Previous research demonstrated that loss of methylation in mCHH islands results in additional loss of transposon CG and CHG methylation (Li et al. 2015a). We compared the methylation levels of CHH, CG, and CHG in the 16 and 31 DMRs. Due to reduced coverage, the methylation levels of many of the 16 suppression-associated DMRs were not available in the *mop1* mutant, but it was possible to examine methylation of 31 enhanced-associated DMRs in the *mop1* mutant. As expected, in the *mop1* mutant, CHH methylation was greatly reduced in these 31 DMRs, as was CG and CHG methylation (Fig. 6E), which echoes previous research (Li et al. 2015a). However, this reduction in CHH methylation did not have a significant effect on the expression of the 31 genes that seemed to be promoted by CHH methylation (Fig. 6F). These data suggest that variations of CHH methylation are a consequence, rather than a cause of variation in gene expression.

Most newly induced CG and CHG DMRs lose methylation, and most newly induced CHH DMRs gain methylation in F1 hybrids

In addition to examining changes in methylation of the parental DMRs, we also investigated the newly induced DMRs in F1 hybrids that were not differentially methylated in the parents. These newly induced DMRs can either gain or lose methylation at an allele relative to both parents (Supplemental Fig. S12A,B). A total of 715 CG, 1,149 CHG, and 3,876 CHH new DMRs were identified (Supplemental Fig. S13). These newly induced DMRs were equally distributed as hyper or hypo DMRs relative to both the B73 and Mo17 genomes (Supplemental Fig. S13C,D),

which is different from the parental DMRs, which were enriched for methylation in the Mo17 genome (Fig. 2B). The newly induced DMRs at CG and CHG sequence contexts largely overlapped with TEs (Supplemental Fig. S13E,F), confirming that TEs are most frequent targets of DNA methylation. Next, we compared the allele specific methylation of these newly induced DMRs. Because the two parents were methylated at the similar levels to those at these newly induced DMRs, we defined the high or low parent the parental allele that was changed in the F1, so the low parent would be the allele whose methylation was reduced in the F1. We found that the majority of newly induced CG (89%, 558 out of 627) and CHG (75%, 918 out of 1,231) DMRs followed the model in Supplemental Fig. S12B, in which one parental allele losses methylation in F1 hybrids (Supplemental Fig. S12D). Interestingly, the majority of newly induced CHH (92%, 2,959 out of 3,230) DMRs followed the model in Supplemental Fig. S12A, in which one parental allele gains methylation in F1 hybrids (Supplemental Fig. S12C), suggesting a distinction between CHH and CG and CHG methylation. We also compared the small RNAs at these newly induced CHH DMRs and did not observe any significant changes in small RNAs between the two parents that had similar methylation levels, or between the hybrids and parents (Supplemental Fig. S14).

Newly triggered methylation at TCM and demethylation at TCdM DMRs in F1 plants can be maintained in the next generation

We next wanted to determine whether the methylation or demethylation triggered in F1 can be maintained in subsequent generations. To test this, we backcrossed WTF1 (Mo17/B73;+/+) and *mop1*F1 (Mo17/B73;*mop1*/*mop1*) with B73 and obtained backcrossed (BC1) plants for WGBS (Fig. 1A). We first analyzed the overall methylation differences between WTF1 and WTBC1. To determine whether changes had been heritably transmitted, we set a cut off for a lack of a change from WTF1 to WTBC1 as <10% change in methylation for CG and CHG and <5% for CHH methylation. We found that approximately 25% of CG and 26% of CHG TCM DMRs met this cut off with less than 10% changes in methylation between F1 and BC1, as did 11% CHH TCM DMRs with less than 5% changes in methylation between F1 and BC1. Interestingly, the CG (35%), CHG (44%) and CHH (38%) TCdM DMRs all had higher percentages of DMRs that met the threshold of differences between F1 and BC1 (Supplemental Tables S7,8), suggesting that TCdM DMRs are more heritable.

To better understand the inheritance of newly acquired DNA methylation, we focused specifically on the inheritance of TCM DMRs. Because all of the sequenced BC1 plants were backcrossed individuals derived from the cross of F1 with B73, we separately analyzed B73 and Mo17 hyper TCM DMRs. For B73 TCM DMRs (Fig. 7A,B, left panels), in which the Mo17 allele has acquired new methylation in F1, BC1 plants could be either homozygous or heterozygous for B73. Among the homozygous BC1 plants, all should have the native level of B73 methylation because it had been the Mo17, not the B73, allele in these DMRs that had changed in the F1. Similarly, BC1 plants that were heterozygous for B73 and the newly converted Mo17 allele would be expected to remain hypermethylated because Mo17 was still in the presence of the B73 allele in these plants (Fig. 7A, left panel). For CG, CHG methylation, this is what we observed. Methylation at these DMRs in all BC1 progeny of B73 TCM DMR plants, both homozygotes and heterozygotes resembled the F1 heterozygotes (Fig. 7C, left panel, and Supplemental Fig. S15C,E). Inheritance of CHH methylation was complicated by the fact that in each case, both alleles in the F1 had elevated methylation relative to parents. Thus, it was possible that each allele or both would return to their original level of methylation. For CHH methylation, the BC1 B73 homozygotes showed levels of methylation similar to the B73 parent, rather than the F1 (Fig. 7D, left panel, and Supplemental Fig. S15G), suggesting that the enhanced methylation in the F1 that resulted from the interaction between B73 and Mo17 had been reduced in the BC1. In the heterozygous BC1s, the overall level of methylation was more similar to the MPV than to the heterozygous F1s (Fig. 7D, left panel, and Supplemental Fig. S15G). This observation suggests that the elevated level of methylation is a consequence of the hybrid genomes, and not just an interaction between alleles, and that the elevated levels of methylation at Mo17 was not heritable.

With respect to heritability, the Mo17 TCM DMRs (Fig. 7A,B, right panels) are more informative. In these cases, the B73 allele has become hypermethylated due to an interaction with the Mo17 allele in F1. The BC1 plants could be either homozygous for B73, in which case one epiallele would remain more methylated if the change at B73 in the F1 were heritable, or heterozygous for Mo17 and B73, in which the B73 allele from the back cross parent should be newly converted to a more methylated state due to interaction with the Mo17 allele in the BC1 generation. Thus, if the change in the B73 in the F1 is heritable, we would expect to see methylation similar to the MPV of the newly converted B73 epiallele and the native B73

epiallele in the homozygotes. In the heterozygotes, we would expect a similar average level of methylation as was observed in the F1 (Fig. 7A, right panel). For CG and CHG methylation, the homozygotes were similar to the MPV of B73 and Mo17, rather than B73, suggesting that changes caused in the F1 plants at B73 were heritably transmitted to the next generation. In contrast, the heterozygotes, which should resemble the F1s because they carry both B73 and Mo17, were also at the MPV (Fig. 7C, right panel, and Supplemental Fig. S15D,F). This suggests that the increase in methylation in B73 due to the presence of Mo17 that we observed in the F1 did not occur in BC1, again suggesting the effects we observed in F1 are not simply due to allelic interactions. For CHH methylation, both the homozygous and heterozygous BC1 plants had methylation at the MPV, rather than the elevated methylation observed in the F1 (Fig. 7D, right panel, and Supplemental Fig. S15H). This indicated that CHH methylation that was added to the Mo17 allele was lost in the BC1, and the presence of the B73 allele did not trigger methylation in Mo17 in this generation.

To determine whether the initiation of TCM requires the presence of MOP1, we also looked at BC1 of mutants. Surprisingly, in all cases described above, the BC1 from the *mop1*F1 mutants was similar to that of the wild type F1s, even for the CHH TCMs. These results suggest that RdDM mediated by MOP1 is not required for *trans*-chromosomal methylation.

Together these data suggest that methylation or demethylation triggered by hybridization can be maintained in the next generation, but that heritability varies depending on the sequence context of the methylated cytosines, and whether new methylation or demethylation is being transmitted. They also show that the elevated methylation we observed in F1 heterozygotes is likely a result of hybridization, rather than simple interaction between alleles.

The *lbl1* mutation has less pronounced effects on DNA methylation

In addition to the canonical RdDM triggered by 24-nt siRNAs, recent research has revealed that 21- to 22-nt siRNAs associated with PTGS can direct RdDM, which has been referred to as non-canonical RdDM or RDR6 RdDM (Nuthikattu et al. 2013; Cuerda-Gil and Slotkin 2016). To determine whether the RDR6-dependent RdDM pathway is involved in the initiation and maintenance of DNA methylation, we performed the similar experiments to those involving *mop1* using the *lbl1* mutants. We crossed *lbl1* heterozygous plants in the B73 and Mo17 backgrounds to each other (B73;*lbl1*/+ × Mo17;*lbl1*/+), and generated hybrid wild type and *lbl1* mutant plants for WGBS (Fig. 8A). Consistent with the wild type controls from the *mop1*

experiment (Fig. 1B and Supplemental Fig. S2), hybridization induced global increases in only CHH methylation (Fig. 8B). However, unlike *mop1*, in which CHH methylation was largely reduced (Fig. 1 and Supplemental Fig. S2), CHH methylation in *lbl1* mutant was not changed globally or near genes or TEs (Supplemental Fig. S16,17). We identified 2,261 CG, 2,427 CHG, and 1,819 CHH parental DRMs as being a consequence of TCM and TCdM in WTF1 (siblings of *lbl1*F1) compared to parents (Supplemental Fig. S18A). As in the *mop1* wild types, the increased methylation at CG and CHG TCM DMRs in WTF1 was primarily due to the increase in methylation of the low-parent allele, and both high- and low-parent alleles at CHH TCM DMRs were increased (Fig. 8C). The decreased methylation at TCdM of all three sequence contexts was due to a reduction of methylation in high-parent allele (Fig. 8D), which is the same as we observed for the WTF1 segregated from the *mop1* plants (Fig. 3C and 3D). On average, *lbl1* mutation did not significantly change the methylation levels for either TCM or TCdM DMRs (Fig. 8C,D). Nevertheless, we still identified 73 CG, 67 CHG, and 293 CHH TCM and TCdM DMRs, in which methylation levels were significantly changed in *lbl1* (Supplemental Fig. S18B-D). We found that changes in methylation of one cytosine context did not result in changes in the other two cytosine contexts at these *lbl1*-affected DMRs (Supplemental Fig. S18E and Supplemental Table S9). Like the distribution of the *mop1*-affected DMRs, *lbl1*-affected CHH DMRs were more enriched in the 2 kb flanking regions of the genes relative to the *lbl1*-affected CG and CHG DMRs (Supplemental Fig. S19). Next, we were interested in the targeted regions of both *lbl1* and *mop1*. We identified 40 CHH TCM DMRs that were affected by both *lbl1* and *mop1* (Supplemental Table S10). These 40 CHH TCM DMRs were enriched near genes (Supplemental Fig. S20). Although both *lbl1* and *mop1* affected these DMRs, *mop1* had a larger effect on them (Fig. 8E and Supplemental Table S11), suggesting that MOP1 is the major component involved in the *de novo* CHH methylation near genes.

Discussion

In this study, we used hybrids as a model system to understand the initiation and maintenance of DNA methylation in maize, with a special focus on CHH methylation, which is abundant in plants, but whose functions are still poorly understood. Our analyses revealed that CHH methylation had some unique features compared to CG and CHG methylation in maize. First, only the level of CHH methylation was increased globally upon hybridization (Fig. 1B). Second,

CHH methylation in maize is largely enriched near genes as mCHH islands (Fig. 1C). This means that most parental CHH DMRs are located within 2 kb flanking regions of genes (Fig. 2E). Third, both the high- and low-parent alleles of CHH TCM DMRs gained methylation in F1 hybrids, while only the low-parent allele gained methylation in CG and CHG TCM DMRs (Fig. 3C,D). Furthermore, although the *mop1* mutation reduced CHH methylation globally (Fig. 1B), it had its biggest effect on the CHH TCM DMRs, and the loss of CHH methylation in *mop1* resulted in additional loss of CHG methylation in these regions (Fig. 4). Next, genetic variation was significantly higher in the demethylated CHH TCdM DMRs than in the methylated CHH TCM DMRs, which was not observed for CG and CHG DMRs (Fig. 5E). Importantly, we also provided evidence that CHH methylation in promoter regions was associated with both the suppressed and enhanced expression of flanking genes (Fig. 6). Genes with enhanced expression by CHH methylation were typically longer, expressed at higher levels, and had higher gene body methylation (Fig. 6D). Finally, we detected an overall lower level of CHH methylation in the backcross individuals (Fig. 7).

Our results demonstrated that small RNAs play a critical role in triggering TCM and TCdM in hybrids and maintaining such interaction in the subsequent generation. An overall reduction of 24-nt siRNAs following hybridization has been documented in a number of plant species including maize (Groszmann et al. 2011; Barber et al. 2012; Greaves et al. 2016). In our analyses, we focused on 24-nt siRNAs specifically at TCM DMRs, and observed no significant difference in the abundance of 24-nt siRNAs between hybrids and the MPV of parents (Fig. 5), as has been seen in Arabidopsis (Zhang et al. 2016). A detailed look at 25 CHH TCM DMRs that had 24-nt siRNAs produced only in one parent showed that 19 (76%) of them had only siRNAs derived from the initially methylated parental allele, despite the fact that both alleles now had CHH methylation. Given that the precursor transcript of 24-nt siRNAs is produced by Pol IV (Matzke and Mosher 2014; Matzke et al. 2015), this data suggests that Pol IV in these F1 plants is only active at one of the two methylated alleles. Our data also showed that CHH TCdM DMRs had significantly higher genetic variation than TCM DMRs, as has been notedly previously (Zhang et al. 2016), which may explain the reduction of methylation at TCdM DMRs given that RdDM relies on the similarity of small RNAs. Small RNAs from the high-parent allele may be too divergent to target the low-parent allele to trigger methylation. However, it is unclear why the

methylation of the high-parent allele is also reduced. Dosage effects may be an explanation (Shi et al. 2020), but that would require further experimental evidence to test it.

Hybridization brings together two divergent genomes into one nucleus, which can induce rapid genomic and epigenomic changes, including gain or loss of DNA fragments, alteration of expression of TEs and genes, changes in splicing cites, activation of endogenous retroviruses, and epigenetic reprogramming (Ishikawa and Kinoshita 2009; Regulski et al. 2013; Qin et al. 2021). It has been hypothesized that hybridization could induce a “genomic shock” that leads to the mobilization of TEs (McClintock 1984). However, evidence for this is mixed and varies between species. Most reports suggest that upregulation of TEs is not a general phenomenon but that some specific TEs may change their expression level upon hybridization, such as the upregulation of *ATHILA* in the crosses of *Arabidopsis thaliana* and *Arabidopsis arenosa* (Josefsson et al. 2006; Gobel et al. 2018). In our study, we observed a genome-wide increase in CHH, but not CG or CHG methylation following hybridization (Fig. 1B). Based on this result, we hypothesize that CHH methylation may buffer the global effects of hybridization on transcriptional activation of TE near genes in maize by transferring silencing information in the form of small RNAs from one genome to the other, resulting in the dramatic increases in CHH *de novo* methylation we observed in the F1 plants. The lack of evidence for the production of new siRNAs from the target loci suggests that in many cases, this methylation is often transient, as is evidenced by the reduced heritability of CHH versus CG and CHG methylation in BC1 plants (Fig. 7). Interestingly, increased levels of CHH methylation were also induced in rice subjected to phosphate starvation (Secco et al. 2015). Because B73 and Mo17 are two inbred lines of maize, rather than two species, hybridization may have subtle effects. The transient nature of the buffering effect, CHH methylation may quickly return to the normal level, as is observed in the WTBC1 plants.

It has been proposed that mCHH islands in maize are the boundaries between highly deep heterochromatin and more active euchromatin to reinforce silencing of TEs located near genes rather than to protect the euchromatic state of the genes (Gent et al. 2013; Li et al. 2015a; Martin et al. 2021). Our study is an ideal model to test this hypothesis because we can examine the effects of presence and absence of mCHH islands on the expression of the same gene in *cis* and in *trans*. As shown in Fig. 6A, a gene in the parent B73 does not have CHH methylation in the promoter region, but obtains methylation after hybridization, which we hypothesize is triggered

in *trans* by small RNAs generated from the Mo17 allele. We demonstrated that out of the 47 CHH TCM DMRs in Mo17 (Mo17 mCHH islands), 16 (34%) were associated with suppressed gene expression, and 31 (66%) were associated with enhanced gene expression (Fig. 6B), indicating that more genes are promoted their expression through gain of CHH methylation in their promoter regions. We next asked why CHH methylation can be positively and negatively associated with the expression of flanking genes. We propose that gene properties and chromatin states of mCHH islands are the primary determinants determining the relationship between CHH methylation and its flanking gene. Our data showed that the 31 genes that seemed to be promoted by CHH methylation were generally longer, expressed higher, and with more gene body methylation than the 16 genes that seemed to be suppressed by CHH methylation (Fig. 6D). This data suggests that more active genes tend to harbor "positive mCHH islands", and lowly expressed genes more likely have "negative mCHH islands", which were significantly enriched for the repressive histone mark H3K27me3 and are depleted with the active mark H3K4me3 (Fig. 6C). We hypothesize that it is the repressive histone mark in the promoter regions suppresses the expression of flanking genes rather than the mCHH islands. Given this assumption, removal of these islands would not have significant effects on flanking gene expression. However, removal of DNA methylation may result in increase of H3K27me3 given that the activity of Polycomb-repressive complex 2, which is involved in catalyzing H3K27me3, is generally anti-correlated with DNA methylation, and likely functions after DNA demethylation (Rodrigues and Zilberman 2015; Batista and Kohler 2020). This probably explains why we observed these 16 genes with "negative mCHH islands" significantly reduced their expression in *mop1* mutants (Fig. 6F). In contrast, the expression of the 31 genes with "positive mCHH islands" were upregulated in the *mop1* mutant although not significantly (Fig. 6F), which supports the hypothesis that mCHH islands do not prevent the spread of heterochromatin silencing of genes (Li et al. 2015a). Rather, these "positive mCHH islands" act as a border to prevent the spread of euchromatin into flanking sequences because loss of the mCHH islands in the *mop1* mutant is accompanied by additional loss of CG and CHG methylation (Fig. 6E) (Li et al. 2015a).

Methods

Genetic material construction and tissue collection

The *mop1* heterozygous plants in the Mo17 background were crossed with the *mop1* heterozygous plants in the B73 background (Mo17;*mop1-1/*+ × B73;*mop1-1/*+) to generate F1 hybrid *mop1* mutants (Mo17/B73;*mop1/mop1*) and their hybrid wildtype siblings (Mo17/B73;+/+) (Fig. 1A). Similarly, *lbl1* heterozygous plants in the B73 and Mo17 backgrounds were crossed to each other (B73;*lbl1*/+ × Mo17;*lbl1*/+) to obtain wild type and *lbl1* F1 hybrid plants (Fig. 8A). Both the *mop1* and *lbl1* mutants were introgressed into the B73 and Mo17 backgrounds for at least seven generations. The F1 plants and the two parental lines (B73 and Mo17) were grown in the Ecology Research Center at Miami University (Oxford, Ohio), and 5-7 cm immature ears were collected for the subsequent whole genome bisulfite sequencing (WGBS), RNA sequencing, and small RNA sequencing with two biological replicates.

Analysis of WGBS data

DNA was isolated from the 5-7 cm immature ears of the two parents (B73 and Mo17), WTF1-*Mop1* (Mo17/B73;+/+, sibling of *mop1*), *mop1*F1 (Mo17/B73;*mop1/mop1*), WTF1-*Lbl1* (B73/Mo17;+/+, sibling of *lbl1*), and *lbl1*F1 (B73/Mo17; *lbl1/lbl1*) using the modified CTAB method. The quality of DNA was examined by Nanodrop. Library construction and subsequent WGBS were performed by Novogene. The raw reads were quality controlled by FastQC. The remaining clean reads from B73, WTF1-*Mop1*, *mop1*F1, WTF1-*Lbl1*, and *lbl1*F1 were mapped to the B73 reference genome (v4) using Bismark under following parameters (-n 2, -I 50, -N 1) (Krueger and Andrews 2011; Jiao et al. 2017). The clean reads from the Mo17 plants were aligned against the SNP replaced Mo17 genome sequences, which were generated by taking the B73 reference sequences and replacing the nucleotides where a SNP identified by the maize Hapmap3 project was present between the two inbreds (Bukowski et al. 2018). Given that treatment of DNA with bisulfite converts cytosine residues to uracil, but leaves 5-methylcytosine residues unaffected, SNPs of C to T and G to A (B73 to Mo17) were excluded from the analysis when considering the B73 allele, and SNPs of T to C and A to G (B73 to Mo17) were excluded from the analysis when considering the Mo17 allele (Li et al. 2023). We kept reads with perfect and unique matches for the two parents, and allowed one mismatch for the hybrids. PCR duplicates were removed using Picardtools. Additional packages including Bismark methylation extractor, bismark2bedGraph and coverage2cytosine under Bismark were used to extract the methylated cytosines, and to count methylated and unmethylated reads (Liu et al. 2021; Yin et al. 2022).

Identification of DMRs between parents

To identify DMRs between parents, we first filtered out the cytosines with less than three mapped reads (Xu et al. 2020). Next, the methylation level of each cytosine was determined by the number of methylated reads out of the total number of reads covering the cytosine (Schultz et al. 2012; Zhao et al. 2017). The software 'metilene' was used for DMR calling between the two parents B73 and Mo17 (Juhling et al. 2016). Specially, a DMR was determined as containing at least eight cytosine sites with the distance of two adjacent cytosine sites <300 bp, and with the average methylation differences in CG and CHG >0.4 and in CHH >0.2 between the two parents (Xu et al. 2020). These DMRs were furthered filtered by the estimated false discovery rates (FDRs) using the Benjamini-Hochberg method (Zhang et al. 2016). We only kept FDRs <0.01 for CG and CHG DMRs, and <0.05 for CHH DMRs (Xu et al. 2020).

Determination of TCM and TCdM in WTF1

To determine the methylation patterns of the parental DMRs in WTF1, we first calculated the methylation levels at the parental DMRs in WTF1. Only DMRs with available data in all the samples were included in the analysis. Fisher's exact test was used to compare the methylation levels of WTF1 to the MPV (middle parent value, the average methylation of the two parents), and the estimated FDRs were generated to adjust *P* values using the Benjamini-Hochberg method (Zhang et al. 2016). DMRs with an FDR <0.05 between WTF1 and the MPV were retained as significantly changed DMRs during hybridization. These DMRs were classified into TCM, which has a significantly higher level of methylation in WTF1 than the MPV, and TCdM, which has a significantly lower level of methylation in WTF1.

To further determine whether the TCM and TCdM were affected by *mop1* or *lbl1* mutation, we first calculated the methylation levels of *mop1*F1 and *lbl1*F1 at TCM and TCdM DMRs. For CG and CHG TCM and TCdM, DMRs with the changes in methylation levels between *mop1*F1 or *lbl1*F1 and WTF1 <-0.4 or >0.4 were considered as significantly affected by the mutation. For CHH TCM and TCdM, DMRs with the changes in methylation levels <-0.2 or >0.2 were considered as significantly changed in the mutants.

Identification of the newly induced DMRs in WTF1

To identify the newly induced DMRs in WTF1 that are not differentially methylated in the parents, we used mpileup in the samtools package and SNPs between B73 and Mo17 to obtain the allele-specific reads from WTF1 (Danecek et al. 2021). Next, these allele-specific reads were used to calculate methylation levels as described above, and 'metilene' was used for DMR

detection between the two alleles in WTF1 (Juhling et al. 2016). The same cutoffs are used for defining new DMRs as for the detection of parental DMRs. The methylation levels of these newly induced DMRs were further compared with the methylation levels of the two parents using Fisher's exact test (FDR <0.05). The DMRs that have similar methylation levels between the two parents but exhibit significantly different methylation levels between the two alleles in WTF1 were defined as new DMRs. The illustration is shown in Supplemental Fig. S12A,B.

Analysis of the inheritance of TCM and TCdM in BC1

We backcrossed WTF1 (Mo17/B73;+/+) and *mop1*F1 (Mo17/B73;*mop1/mop1*) with B73 (Mo17/B73;+/+ × B73 and Mo17/B73;*mop1/mop1* × B73) to generate the BC1 generation. We collected 5-7 cm immature ears from eight WTBC1 plants and eight *mop1*-derived-BC1 plants for WGBS (Fig. 1A). The methylation analysis for BC1 is the same as that for parents and WTF1. Next, we compared the methylation levels at the TCM and TCdM DMRs among WTBC1, *mop1*-derived-BC1, WTF1, *mop1*F1, and parents. The "intersect" function in BEDTools was used to access all the cytosines in BC1 that are at the TCM and TCdM DMRs, and these cytosines were used to calculate the average methylation levels across all the BC1 individuals in those regions. As shown in Fig. 8A,B, because we only sequenced the BC1 individuals derived from the backcrosses of F1 and B73, we separated B73/B73 homozygous and B73/Mo17 heterozygous genotypes at each TCM in BC1 using samtools mpileup and the SNPs between B73 and Mo17 (Bukowski et al. 2018; Danecek et al. 2021), same as what we did for the determination of allele specific reads in F1.

Distribution analysis of DMRs in different genomic locations

To classify the DMRs in different genomic locations, we compared the locations of the DMRs with gene and transposable element annotations, which were downloaded from MaizeGDB, https://www.maizegdb.org/, using intersect function in BEDTools (Quinlan and Hall 2010). If one DMR is dropped to two different types of annotation, we followed the order gene bodies, 2 kb upstream of genes, 2kb downstream of genes, TEs, and unclassified regions. DMRs in the 2 kb up and downstream regions of genes were further separated into those with and without TEs depending on whether there is a TE insertion in the 2 kb flanking regions.

Analysis of small RNA-seq data

The same genetic materials for B73 and Mo17, WTF1, and *mop1*F1 were used for small RNA sequencing with two biological replicates. The raw reads were quality controlled by FastQC. The clean reads were aligned against the Rfam database (v14.6) to remove rRNAs, tRNAs, snRNAs, and snoRNAs (Yin et al. 2022). The remaining reads with the length of 18-26 nt were retained for further mapping to the genomes. The reads from B73, WTF1, and *mop1*F1 were mapped to the B73 reference genome (v4), and the reads from Mo17 were mapped to the SNP replaced Mo17 genome sequences using bowtie (Langmead et al. 2009; Jiao et al. 2017), as was done for our methylation analysis. For the parents, only perfectly and uniquely mapped reads were kept, and one mismatch was allowed for the F1 hybrids. The small RNA values were adjusted to total abundance of all mature microRNAs following the previous research to remove the artificial increase of 22-nt siRNAs in *mop1* mutants caused by normalization (Nobuta et al. 2008). The intersect module in BEDTools was used to compare the mapping results (sam files) to the positions of DMRs to obtain the 24-nt small RNA reads that are in the DMRs (Quinlan and Hall 2010). These 24-nt small RNAs were used to calculate the expression of small RNAs of the DMRs. To access allele specific small RNA expression, samtools mpileup and SNPs at small RNAs between B73 and Mo17 were used (Danecek et al. 2021).

Analysis of mRNA-seq data

The mRNA from the same genetic materials were sequenced with two biological replicates. The raw reads were quality controlled by FastQC, and the low-quality reads and the adapter sequences were removed by Trimmomatic (Bolger et al. 2014). We mapped the cleaned reads of B73, WTF1, and *mop1*F1 to the B73 reference genome (v4) (Jiao et al. 2017), and the reads from Mo17 to the SNP replaced Mo17 genome that was generated by replacing the B73 genome with the SNPs between Mo17 and B73 using Hisat2 with one mismatch (Kim et al. 2019). Next, HTSeq-count was used to calculate the total number of reads of each gene (Putri et al. 2022). These values were loaded to DESeq2 to identify genes that were differentially expressed between WTF1 and parents, and between WTF1 and *mop1*F1 (Love et al. 2014). To determine allele specific expression of each gene in F1, the mpileup function in samtools and SNPs between B73 and Mo17 were used to access allele specific reads (Danecek et al. 2021), which were further used in DESeq2 to identify differential expression of the two alleles (Love et al. 2014).

Accession Numbers

The raw and processed data of whole genome bisulfite, mRNA and small RNA sequencing presented in this study have been deposited in NCBI Gene Expression Omnibus under the accession number GSE222155. All the other data that support the findings of this study are available within the paper and its Supplemental Data.

Competing interest statement

The authors declare no competing interests.

Acknowledgements

We are grateful to Nathan M Springer and Karen M. McGinnis for critical reading of the manuscript. We thank Ohio Supercomputer Center for providing us the computational resources to perform the analysis. This work was supported by the National Institute of General Medical Sciences of the National Institutes of Health under Award Number R15GM135874 and the National Science Foundation (Plant Genome Research Program) under Award Number IOS2306220 to M.Z.

Author contributions

M.Z. designed the experiments. B.L. and M.Z. prepared the research materials for sequencing. B.L., D.Y., D.W., and M.Z. analyzed the data. B.L. and M.Z. wrote the original draft, and C.L., J.W., and D.L. reviewed and edited the manuscript.

References

Alleman M, Sidorenko L, McGinnis K, Seshadri V, Dorweiler JE, White J, Sikkink K, Chandler VL. 2006. An RNA-dependent RNA polymerase is required for paramutation in maize. *Nature* **442**: 295-298.

Arteaga-Vazquez MA, Chandler VL. 2010. Paramutation in maize: RNA mediated trans-generational gene silencing. *Curr Opin Genet Dev* **20**: 156-163.

Barber WT, Zhang W, Win H, Varala KK, Dorweiler JE, Hudson ME, Moose SP. 2012. Repeat associated small RNAs vary among parents and following hybridization in maize. *Proc Natl Acad Sci U S A* **109**: 10444-10449.

Batista RA, Kohler C. 2020. Genomic imprinting in plants-revisiting existing models. *Genes Dev* **34**: 24-36.

Bolger AM, Lohse M, Usadel B. 2014. Trimmomatic: a flexible trimmer for Illumina sequence data. *Bioinformatics* **30**: 2114-2120.

Bukowski R, Guo X, Lu Y, Zou C, He B, Rong Z, Wang B, Xu D, Yang B, Xie C et al. 2018. Construction of the third-generation Zea mays haplotype map. *Gigascience* **7**: 1-12.

Cao S, Wang L, Han T, Ye W, Liu Y, Sun Y, Moose SP, Song Q, Chen ZJ. 2022. Small RNAs mediate transgenerational inheritance of genome-wide trans-acting epialleles in maize. *Genome Biol* **23**: 53.

Chodavarapu RK, Feng S, Ding B, Simon SA, Lopez D, Jia Y, Wang GL, Meyers BC, Jacobsen SE, Pellegrini M. 2012. Transcriptome and methylome interactions in rice hybrids. *Proc Natl Acad Sci U S A* **109**: 12040-12045.

Cuerda-Gil D, Slotkin RK. 2016. Non-canonical RNA-directed DNA methylation. *Nat Plants* **2**: 16163.

Danecek P, Bonfield JK, Liddle J, Marshall J, Ohan V, Pollard MO, Whitwham A, Keane T, McCarthy SA, Davies RM et al. 2021. Twelve years of SAMtools and BCFtools. *Gigascience* **10**.

Erdmann RM, Picard CL. 2020. RNA-directed DNA Methylation. *PLoS Genet* **16**: e1009034.

Gent JI, Ellis NA, Guo L, Harkess AE, Yao Y, Zhang X, Dawe RK. 2013. CHH islands: de novo DNA methylation in near-gene chromatin regulation in maize. *Genome Res* **23**: 628-637.

Gent JI, Madzima TF, Bader R, Kent MR, Zhang X, Stam M, McGinnis KM, Dawe RK. 2014. Accessible DNA and relative depletion of H3K9me2 at maize loci undergoing RNA-directed DNA methylation. *Plant Cell* **26**: 4903-4917.

Gobel U, Arce AL, He F, Rico A, Schmitz G, de Meaux J. 2018. Robustness of Transposable Element Regulation but No Genomic Shock Observed in Interspecific Arabidopsis Hybrids. *Genome Biol Evol* **10**: 1403-1415.

Greaves IK, Eichten SR, Groszmann M, Wang A, Ying H, Peacock WJ, Dennis ES. 2016. Twenty-four-nucleotide siRNAs produce heritable trans-chromosomal methylation in F1 Arabidopsis hybrids. *Proc Natl Acad Sci U S A* **113**: E6895-E6902.

Greaves IK, Gonzalez-Bayon R, Wang L, Zhu A, Liu PC, Groszmann M, Peacock WJ, Dennis ES. 2015. Epigenetic Changes in Hybrids. *Plant Physiol* **168**: 1197-1205.

Greaves IK, Groszmann M, Wang A, Peacock WJ, Dennis ES. 2014. Inheritance of Trans Chromosomal Methylation patterns from Arabidopsis F1 hybrids. *Proc Natl Acad Sci U S A* **111**: 2017-2022.

Greaves IK, Groszmann M, Ying H, Taylor JM, Peacock WJ, Dennis ES. 2012. Trans chromosomal methylation in Arabidopsis hybrids. *Proc Natl Acad Sci U S A* **109**: 3570-3575.

Groszmann M, Greaves IK, Albertyn ZI, Scofield GN, Peacock WJ, Dennis ES. 2011. Changes in 24-nt siRNA levels in Arabidopsis hybrids suggest an epigenetic contribution to hybrid vigor. *Proc Natl Acad Sci U S A* **108**: 2617-2622.

He G, Chen B, Wang X, Li X, Li J, He H, Yang M, Lu L, Qi Y, Wang X et al. 2013. Conservation and divergence of transcriptomic and epigenomic variation in maize hybrids. *Genome Biol* **14**: R57.

He G, Zhu X, Elling AA, Chen L, Wang X, Guo L, Liang M, He H, Zhang H, Chen F et al. 2010. Global epigenetic and transcriptional trends among two rice subspecies and their reciprocal hybrids. *Plant Cell* **22**: 17-33.

He XJ, Chen T, Zhu JK. 2011. Regulation and function of DNA methylation in plants and animals. *Cell Res* **21**: 442-465.

Hollick JB. 2017. Paramutation and related phenomena in diverse species. *Nat Rev Genet* **18**: 5-23.

Hollister JD, Gaut BS. 2009. Epigenetic silencing of transposable elements: A trade-off between reduced transposition and deleterious effects on neighboring gene expression. *Genome Res* **19**: 1419-1428.

Ishikawa R, Kinoshita T. 2009. Epigenetic programming: the challenge to species hybridization. *Mol Plant* **2**: 589-599.

Jiao Y, Peluso P, Shi J, Liang T, Stitzer MC, Wang B, Campbell MS, Stein JC, Wei X, Chin CS et al. 2017. Improved maize reference genome with single-molecule technologies. *Nature* **546**: 524-527.

Josefsson C, Dilkes B, Comai L. 2006. Parent-dependent loss of gene silencing during interspecies hybridization. *Curr Biol* **16**: 1322-1328.

Juhling F, Kretzmer H, Bernhart SH, Otto C, Stadler PF, Hoffmann S. 2016. metilene: fast and sensitive calling of differentially methylated regions from bisulfite sequencing data. *Genome Res* **26**: 256-262.

Junaid A, Kumar H, Rao AR, Patil AN, Singh NK, Gaikwad K. 2018. Unravelling the epigenomic interactions between parental inbreds resulting in an altered hybrid methylome in pigeonpea. *DNA Res* **25**: 361-373.

Kenan-Eichler M, Leshkowitz D, Tal L, Noor E, Melamed-Bessudo C, Feldman M, Levy AA. 2011. Wheat hybridization and polyploidization results in deregulation of small RNAs. *Genetics* **188**: 263-272.

Kim D, Paggi JM, Park C, Bennett C, Salzberg SL. 2019. Graph-based genome alignment and genotyping with HISAT2 and HISAT-genotype. *Nat Biotechnol* **37**: 907-915.

Krueger F, Andrews SR. 2011. Bismark: a flexible aligner and methylation caller for Bisulfite-Seq applications. *Bioinformatics* **27**: 1571-1572.

Langmead B, Trapnell C, Pop M, Salzberg SL. 2009. Ultrafast and memory-efficient alignment of short DNA sequences to the human genome. *Genome Biol* **10**: R25.

Law JA, Jacobsen SE. 2010. Establishing, maintaining and modifying DNA methylation patterns in plants and animals. *Nat Rev Genet* **11**: 204-220.

Lewsey MG, Hardcastle TJ, Melnyk CW, Molnar A, Valli A, Urich MA, Nery JR, Baulcombe DC, Ecker JR. 2016. Mobile small RNAs regulate genome-wide DNA methylation. *Proc Natl Acad Sci U S A* **113**: E801-810.

Li Q, Eichten SR, Hermanson PJ, Springer NM. 2014. Inheritance patterns and stability of DNA methylation variation in maize near-isogenic lines. *Genetics* **196**: 667-676.

Li Q, Gent JI, Zynda G, Song J, Makarevitch I, Hirsch CD, Hirsch CN, Dawe RK, Madzima TF, McGinnis KM et al. 2015a. RNA-directed DNA methylation enforces boundaries between heterochromatin and euchromatin in the maize genome. *Proc Natl Acad Sci U S A* **112**: 14728-14733.

Li Q, Song J, West PT, Zynda G, Eichten SR, Vaughn MW, Springer NM. 2015b. Examining the Causes and Consequences of Context-Specific Differential DNA Methylation in Maize. *Plant Physiol* **168**: 1262-1274.

Li T, Yin L, Stoll CE, Lisch D, Zhao M. 2023. Conserved noncoding sequences and de novo Mutator insertion alleles are imprinted in maize. *Plant Physiol* **191**: 299-316.

Liu B, Iwata-Otsubo A, Yang D, Baker RL, Liang C, Jackson SA, Liu S, Ma J, Zhao M. 2021. Analysis of CACTA transposase genes unveils the mechanism of intron loss and distinct small RNA silencing pathways underlying divergent evolution of Brassica genomes. *Plant J* **105**: 34-48.

Love MI, Huber W, Anders S. 2014. Moderated estimation of fold change and dispersion for RNA-seq data with DESeq2. *Genome Biol* **15**: 550.

Ma X, Xing F, Jia Q, Zhang Q, Hu T, Wu B, Shao L, Zhao Y, Zhang Q, Zhou DX. 2021. Parental variation in CHG methylation is associated with allelic-specific expression in elite hybrid rice. *Plant Physiol* **186**: 1025-1041.

Martin GT, Seymour DK, Gaut BS. 2021. CHH Methylation Islands: A Nonconserved Feature of Grass Genomes That Is Positively Associated with Transposable Elements but Negatively Associated with Gene-Body Methylation. *Genome Biol Evol* **13**.

Matzke MA, Kanno T, Matzke AJ. 2015. RNA-Directed DNA Methylation: The Evolution of a Complex Epigenetic Pathway in Flowering Plants. *Annu Rev Plant Biol* **66**: 243-267.

Matzke MA, Mosher RA. 2014. RNA-directed DNA methylation: an epigenetic pathway of increasing complexity. *Nat Rev Genet* **15**: 394-408.

McClintock B. 1984. The significance of responses of the genome to challenge. *Science* **226**: 792-801.

Muyle AM, Seymour DK, Lv Y, Huettel B, Gaut BS. 2022. Gene Body Methylation in Plants: Mechanisms, Functions, and Important Implications for Understanding Evolutionary Processes. *Genome Biol Evol* **14**.

Nobuta K, Lu C, Shrivastava R, Pillay M, De Paoli E, Accerbi M, Arteaga-Vazquez M, Sidorenko L, Jeong DH, Yen Y et al. 2008. Distinct size distribution of endogeneous siRNAs in maize: Evidence from deep sequencing in the mop1-1 mutant. *Proc Natl Acad Sci U S A* **105**: 14958-14963.

Nuthikattu S, McCue AD, Panda K, Fultz D, DeFraia C, Thomas EN, Slotkin RK. 2013. The initiation of epigenetic silencing of active transposable elements is triggered by RDR6 and 21-22 nucleotide small interfering RNAs. *Plant Physiol* **162**: 116-131.

Panda K, Ji L, Neumann DA, Daron J, Schmitz RJ, Slotkin RK. 2016. Full-length autonomous transposable elements are preferentially targeted by expression-dependent forms of RNA-directed DNA methylation. *Genome Biol* **17**: 170.

Putri GH, Anders S, Pyl PT, Pimanda JE, Zanini F. 2022. Analysing high-throughput sequencing data in Python with HTSeq 2.0. *Bioinformatics* **38**: 2943-2945.

Qin J, Mo R, Li H, Ni Z, Sun Q, Liu Z. 2021. The Transcriptional and Splicing Changes Caused by Hybridization Can Be Globally Recovered by Genome Doubling during Allopolyploidization. *Mol Biol Evol* **38**: 2513-2519.

Quinlan AR, Hall IM. 2010. BEDTools: a flexible suite of utilities for comparing genomic features. *Bioinformatics* **26**: 841-842.

Regulski M, Lu Z, Kendall J, Donoghue MT, Reinders J, Llaca V, Deschamps S, Smith A, Levy D, McCombie WR et al. 2013. The maize methylome influences mRNA splice sites and reveals widespread paramutation-like switches guided by small RNA. *Genome Res* **23**: 1651-1662.

Ricci WA, Lu Z, Ji L, Marand AP, Ethridge CL, Murphy NG, Noshay JM, Galli M, Mejia-Guerra MK, Colome-Tatche M et al. 2019. Widespread long-range cis-regulatory elements in the maize genome. *Nat Plants* **5**: 1237-1249.

Rodrigues JA, Zilberman D. 2015. Evolution and function of genomic imprinting in plants. *Genes Dev* **29**: 2517-2531.

Schmitz RJ, He Y, Valdes-Lopez O, Khan SM, Joshi T, Urich MA, Nery JR, Diers B, Xu D, Stacey G et al. 2013. Epigenome-wide inheritance of cytosine methylation variants in a recombinant inbred population. *Genome Res* **23**: 1663-1674.

Schmitz RJ, Schultz MD, Lewsey MG, O'Malley RC, Urich MA, Libiger O, Schork NJ, Ecker JR. 2011. Transgenerational epigenetic instability is a source of novel methylation variants. *Science* **334**: 369-373.

Schultz MD, Schmitz RJ, Ecker JR. 2012. 'Leveling' the playing field for analyses of single-base resolution DNA methylomes. *Trends Genet* **28**: 583-585.

Secco D, Wang C, Shou H, Schultz MD, Chiarenza S, Nussaume L, Ecker JR, Whelan J, Lister R. 2015. Stress induced gene expression drives transient DNA methylation changes at adjacent repetitive elements. *Elife* **4**.

Shen H, He H, Li J, Chen W, Wang X, Guo L, Peng Z, He G, Zhong S, Qi Y et al. 2012. Genome-wide analysis of DNA methylation and gene expression changes in two Arabidopsis ecotypes and their reciprocal hybrids. *Plant Cell* **24**: 875-892.

Shi X, Chen C, Yang H, Hou J, Ji T, Cheng J, Veitia RA, Birchler JA. 2020. The Gene Balance Hypothesis: Epigenetics and Dosage Effects in Plants. *Methods Mol Biol* **2093**: 161-171.

Shivaprasad PV, Dunn RM, Santos BA, Bassett A, Baulcombe DC. 2012. Extraordinary transgressive phenotypes of hybrid tomato are influenced by epigenetics and small silencing RNAs. *EMBO J* **31**: 257-266.

Stroud H, Do T, Du J, Zhong X, Feng S, Johnson L, Patel DJ, Jacobsen SE. 2014. Non-CG methylation patterns shape the epigenetic landscape in Arabidopsis. *Nat Struct Mol Biol* **21**: 64-72.

Takuno S, Gaut BS. 2012. Body-methylated genes in Arabidopsis thaliana are functionally important and evolve slowly. *Mol Biol Evol* **29**: 219-227.

Wu L, Mao L, Qi Y. 2012. Roles of dicer-like and argonaute proteins in TAS-derived small interfering RNA-triggered DNA methylation. *Plant Physiol* **160**: 990-999.

Xu G, Lyu J, Li Q, Liu H, Wang D, Zhang M, Springer NM, Ross-Ibarra J, Yang J. 2020. Evolutionary and functional genomics of DNA methylation in maize domestication and improvement. *Nat Commun* **11**: 5539.

Yin L, Xu G, Yang J, Zhao M. 2022. The Heterogeneity in the Landscape of Gene Dominance in Maize is Accompanied by Unique Chromatin Environments. *Mol Biol Evol* **39**.

Zhang Q, Wang D, Lang Z, He L, Yang L, Zeng L, Li Y, Zhao C, Huang H, Zhang H et al. 2016. Methylation interactions in Arabidopsis hybrids require RNA-directed DNA methylation and are influenced by genetic variation. *Proc Natl Acad Sci U S A* **113**: E4248-4256.

Zhao M, Ku JC, Liu B, Yang D, Yin L, Ferrell TJ, Stoll CE, Guo W, Zhang X, Wang D et al. 2021. The mop1 mutation affects the recombination landscape in maize. *Proc Natl Acad Sci U S A* **118**.

Zhao M, Zhang B, Lisch D, Ma J. 2017. Patterns and Consequences of Subgenome Differentiation Provide Insights into the Nature of Paleopolyploidy in Plants. *Plant Cell* **29**: 2974-2994.

Zilberman D, Gehring M, Tran RK, Ballinger T, Henikoff S. 2007. Genome-wide analysis of Arabidopsis thaliana DNA methylation uncovers an interdependence between methylation and transcription. *Nat Genet* **39**: 61-69.

Figure legends

Figure 1. CHH methylation level is globally increased in hybrids.

(*A*) Genetic strategy to construct wild type F1 (WTF1), *mop1* mutant F1 (*mop1*F1), and backcross1 (BC1). (*B*) The distribution of CG, CHG, and CHH methylation on chromosome 5. Methylation levels were measured in 1 Mb windows with 500 kb shift. (*C*) Patterns of methylation in and flanking genes. (*D*) Patterns of methylation in and flanking TEs. DNA methylation levels were calculated in 50 bp windows in the 3 kb upstream and downstream regions of the genes/transposable elements (TEs). Each gene/TE sequence was divided into 40 equally sized bins to measure the gene/TE body methylation. Bin sizes differ from gene/TE to gene/TE because of the different lengths of genes/TEs. The methylation levels of TEs were orientated into proximal and distal ends depending on the location of genes flanking the TEs. Methylation for each sample was calculated as the proportion of methylated C over total C in each sequence context (CG, CHG, and CHH, where H = A, T, or C) averaged for each window. The average methylation levels were determined by combining two biological replicates for each genotype.

Figure 2. Parental CHH DMRs are largely located within 2 kb flanking regions of genes.

(*A*) Definition of B73 hyper DMRs (higher methylation in B73) and Mo17 hyper DMRs (higher methylation in Mo17) between parents. Red, green, and blue dots represent CG, CHG, and CHH methylation, respectively. (*B*) B73 has more CG and CHG hyper DMRs, and Mo17 has more hyper CHH DMRs. (*C*) B73 has higher methylation levels at CG and CHG DMRs, and Mo17 has higher methylation levels at CHH DMRs. (*D*) CG and CHG DMRs were more overlapped with each other than each was with CHH DMRs. (*E*) The distribution of CG, CHG and CHH parental DMRs. 2 kb up and downstream of genes overlapping TEs indicates the DMRs overlap TEs within the 2 kb flanking regions of genes. (*F*) The types of TEs at the categories of 2 kb up and downstream of genes overlapping TEs in (*E*). DMRs, differentially methylated regions.

Figure 3. The levels of CHH methylation of both high- and low-parent alleles are increased at TCM DMRs in the F1 hybrids.

(*A*) Identification of TCM, TCdM, and unchanged (NC) DMRs between WTF1 and parents. (*B*) Comparisons of CG, CHG and CHH methylation at TCM DMRs in parents, WTF1 and *mop1*F1.

(*C*) Comparisons of CG, CHG and CHH methylation at TCdM DMRs in parents, WTF1 and *mop1*F1. HP, high parent (parent with higher methylation). HA, high-parent allele in F1. LP, low parent (parent with lower methylation). LA, low-parent allele in F1. Average means the average between the two parents, or between the two alleles in WTF1 and *mop1*F1. DMRs, differentially methylated regions. TCM, *trans*-chromosomal methylation. TCdM, *trans*-chromosomal demethylation.

Figure 4. The *mop*1 mutation primarily removes the methylation of CHH TCM DMRs.
(*A*) Number of CG, CHG and CHH TCM DMRs affected by the *mop1* mutation. (*B*) Comparison of methylation levels at the *mop1*-affected CG, CHG, and CHH TCM DMRs. (*C*) Number of CG, CHG and CHH TCdM DMRs affected by the *mop1* mutation. (*D*) Examination of the methylation changes in the other two cytosine contexts at the *mop1*-affected CG, CHG, and CHH TCM DMRs. The top panel shows the methylation changes in CHG and CHH sequence contexts at the 99 *mop1*-affected CG TCM DMRs. The middle panel shows the methylation changes in CG and CHH sequence contexts at the 144 *mop1*-affected CHG TCM DMRs. The bottom panel shows the methylation changes in CG and CHG sequence contexts at the 1031 *mop1*-affected CHH TCM DMRs. HP, high parent (parent with higher methylation). LP, low parent (parent with lower methylation). MPV, the middle parent value. DMRs, differentially methylated regions. TCM, *trans*-chromosomal methylation. TCdM, *trans*-chromosomal demethylation.

Figure 5. Small RNAs produced from one parent are sufficient to trigger new methylation of the other allele in hybrids.
(*A*) Two hypothetical models of small RNA biogenesis in F1 at CHH TCM. (*B*) Expression values of small RNAs in parents, WTF1 and *mop1*F1. TPM, transcripts per million uniquely mapped reads. The small RNA values were adjusted to total abundance of all mature microRNAs following the previous research (Nobuta et al., 2008). (*C*) The abundance of 24 nt small interfering RNA (siRNAs) at the *mop1*-affected CHH TCM DMRs. HP, high parent (parent with higher methylation). LP, low parent (parent with lower methylation). MPV, the middle parent value. RPKM, 24 nt siRNA reads per kilobase (DMR length) per million uniquely mapped reads. (*D*) Ratios of 24 nt siRNAs of high parent to low parent, and of high-parent allele to low-parent allele at the *mop1*-affected CHH TCM DMRs. (*E*) Number of single nucleotides polymorphisms

(SNPs) between TCM and TCdM. **, $P < 0.01$, *, $P < 0.05$, Student's *t* test. DMRs, differentially methylated regions. TCM, *trans*-chromosomal methylation. TCdM, *trans*-chromosomal demethylation.

Figure 6. CHH methylation is associated with both suppressed and enhanced expression of their flanking genes.

(*A*) Two possible scenarios of the effects of CHH methylation on gene expression. Here only shows the examples of Mo17 CHH TCM DMRs. (*B*) Number of genes identified based on the models in (*A*). The ratios of expression values of Mo17 to B73 between the parents and WTF1 were used to determine the scenarios. (*C*) Histone modification of 16 CHH TCM DMRs that are associated with the suppressed expression of flanking genes and 31 CHH TCM DMRs that are associated with the enhanced expression of flanking genes. **, $P < 0.01$, Student's *t* test. (*D*) Gene properties of the 16 suppressed and 31 enhanced genes. **, $P < 0.01$, *, $P < 0.05$, Student's *t* test. (*E*) Methylation changes in *mop1* mutants at the 31 CHH TCM DMRs that are associated with the enhanced expression of flanking genes. **, $P < 0.01$, Student's paired *t* test. (*F*) Gene expression changes of the 16 suppressed and 31 enhanced genes in *mop1* mutants. *, $P < 0.01$, Student's paired *t* test. DMRs, differentially methylated regions. TCM, *trans*-chromosomal methylation.

Figure 7. Newly triggered methylation at TCM and demethylation at TCdM DMRs in F1 plants can be maintained in the next generation. (*A*) Hypothetical models assuming maintenance of CG and CHG TCM DMRs. (*B*) Hypothetical models assuming maintenance of CHH TCM DMRs. (*C*) Methylation changes of CG and CHG TCM DMRs. (*D*) Methylation changes of CHH TCM DMRs. (*E*) Distribution and methylation levels of two examples of Mo17 CHH TCM DMRs. DMRs, differentially methylated regions. TCM, *trans*-chromosomal methylation. Homo, homozygous. Hetero, heterozygous.

Figure 8. The *lbl1* mutation has less effects on DNA methylation.

(*A*) Genetic strategy to obtain the wild type F1 (WTF1) and *lbl1* mutant F1 (*lbl1*F1). (*B*) The distribution of CG, CHG, and CHH methylation on chromosome 5. Methylation levels were measured in 1 Mb windows with 500 kb shift. (*C*) Comparisons of CG, CHG and CHH

methylation at TCM DMRs in parents, WTF1 and *lbl1*F1. (*D*) Comparisons of CG, CHG and CHH methylation at TCdM DMRs in parents, WTF1 and *lbl1*F1. (E) CHH TCM DMRs affected by both *mop*1 and *lbl1* mutations. HP, high parent (parent with higher methylation). HA, high-parent allele in F1. LP, low parent (parent with lower methylation). LA, low-parent allele in F1. Average means the average between the two parents, or between the two alleles in WTF1 and *lbl1*F1. DMRs, differentially methylated regions. TCM, *trans*-chromosomal methylation. TCdM, *trans*-chromosomal demethylation.

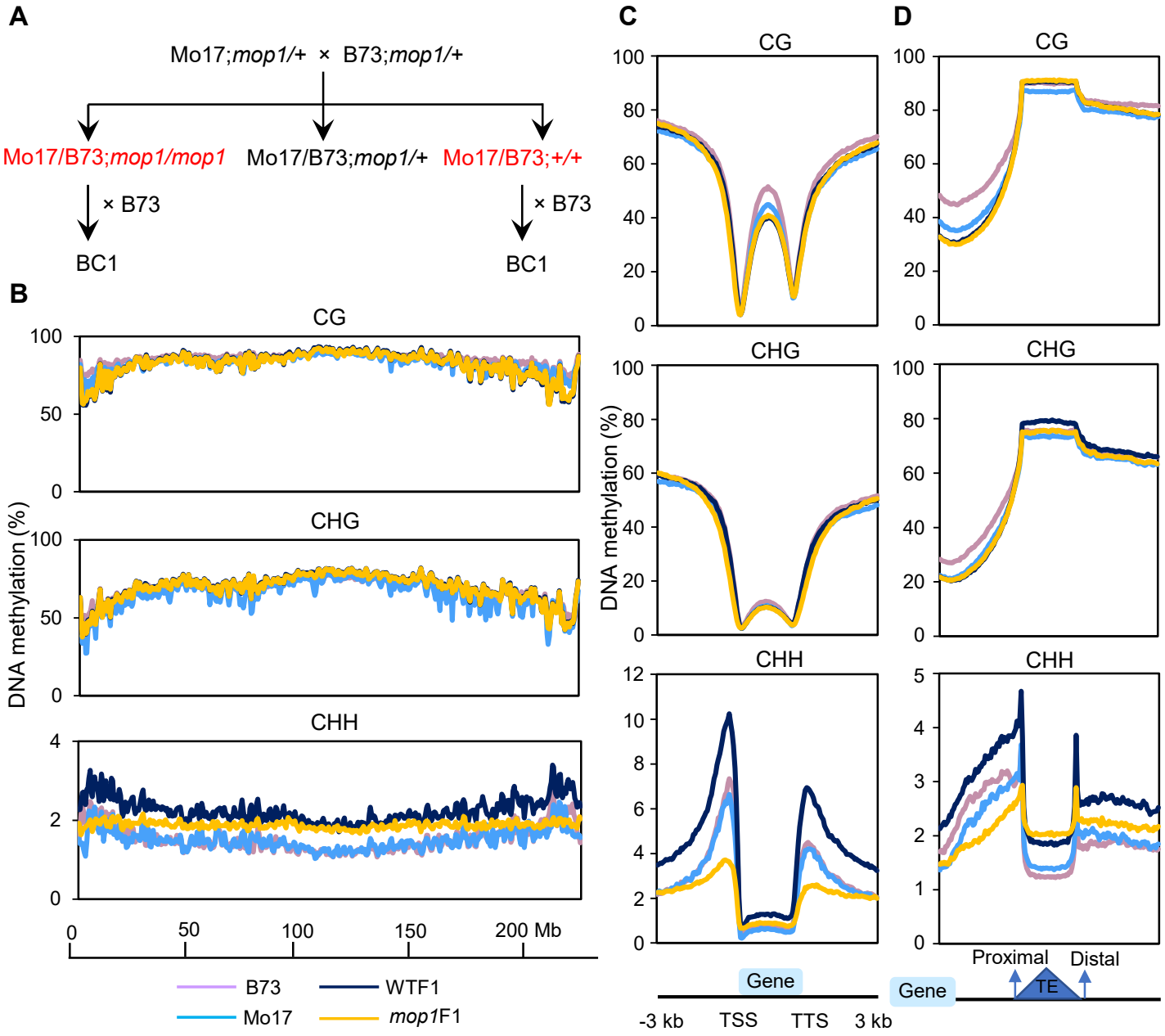

Figure 1. CHH methylation level is globally increased in hybrids.
(*A*) Genetic strategy to construct wild type F1 (WTF1), *mop1* mutant F1 (*mop1*F1), and backcross1 (BC1). (*B*) The distribution of CG, CHG, and CHH methylation on chromosome 5. Methylation levels were measured in 1 Mb windows with 500 kb shift. (*C*) Patterns of methylation in and flanking genes. (*D*) Patterns of methylation in and flanking TEs. DNA methylation levels were calculated in 50 bp windows in the 3 kb upstream and downstream regions of the genes/transposable elements (TEs). Each gene/TE sequence was divided into 40 equally sized bins to measure the gene/TE body methylation. Bin sizes differ from gene/TE to gene/TE because of the different lengths of genes/TEs. The methylation levels of TEs were orientated into proximal and distal ends depending on the location of genes flanking the TEs. Methylation for each sample was calculated as the proportion of methylated C over total C in each sequence context (CG, CHG, and CHH, where H = A, T, or C) averaged for each window. The average methylation levels were determined by combining two biological replicates for each genotype.

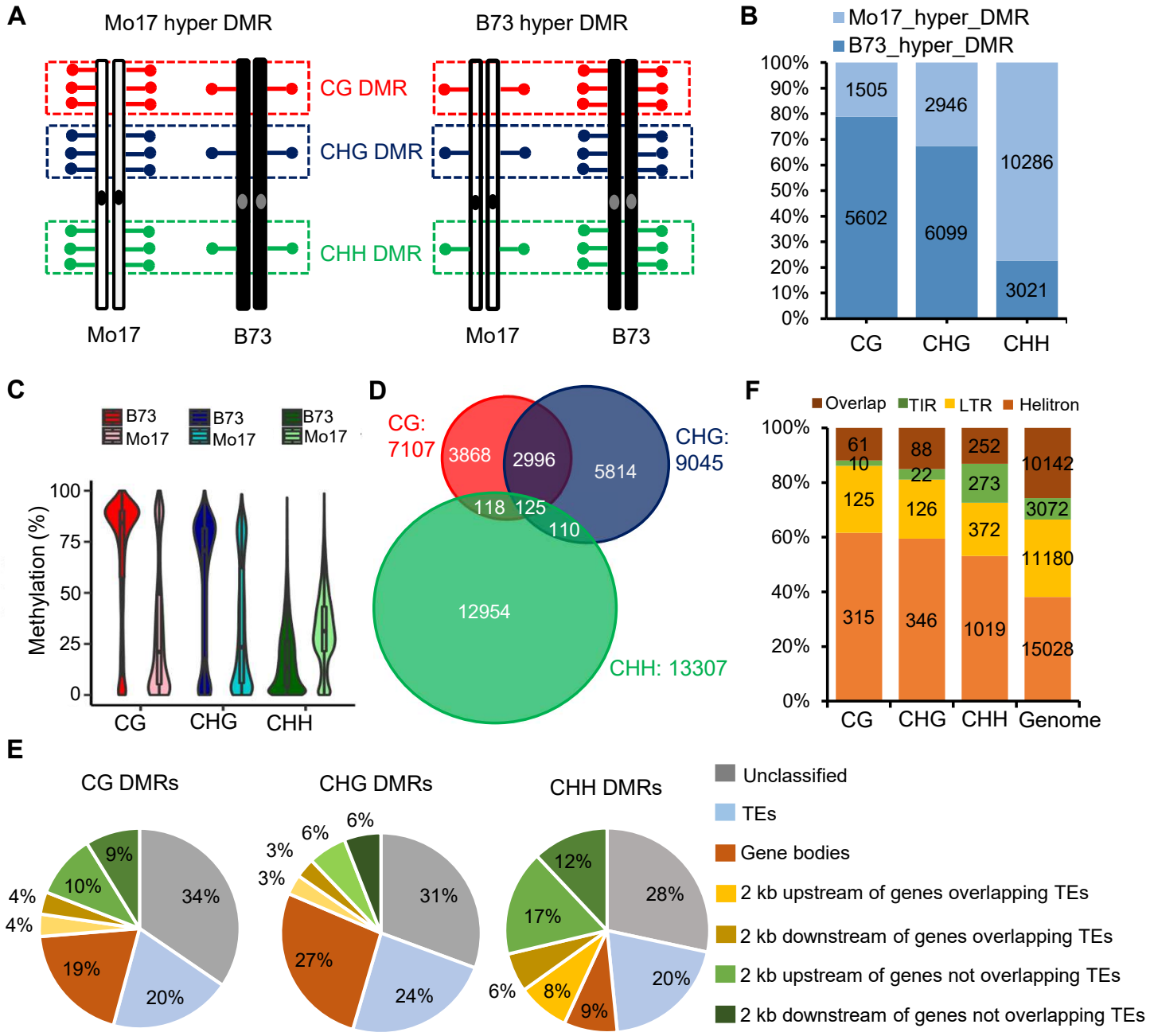

Figure 2. Parental CHH DMRs are largely located within 2 kb flanking regions of genes.
(*A*) Definition of B73 hyper DMRs (higher methylation in B73) and Mo17 hyper DMRs (higher methylation in Mo17) between parents. Red, green, and blue dots represent CG, CHG, and CHH methylation, respectively. (*B*) B73 has more CG and CHG hyper DMRs, and Mo17 has more hyper CHH DMRs. (*C*) B73 has higher methylation levels at CG and CHG DMRs, and Mo17 has higher methylation levels at CHH DMRs. (*D*) CG and CHG DMRs were more overlapped with each other than each was with CHH DMRs. (*E*) The distribution of CG, CHG and CHH parental DMRs. 2 kb up and downstream of genes overlapping TEs indicates the DMRs overlap TEs within the 2 kb flanking regions of genes. (*F*) The types of TEs at the categories of 2 kb up and downstream of genes overlapping TEs in (*E*). DMRs, differentially methylated regions.

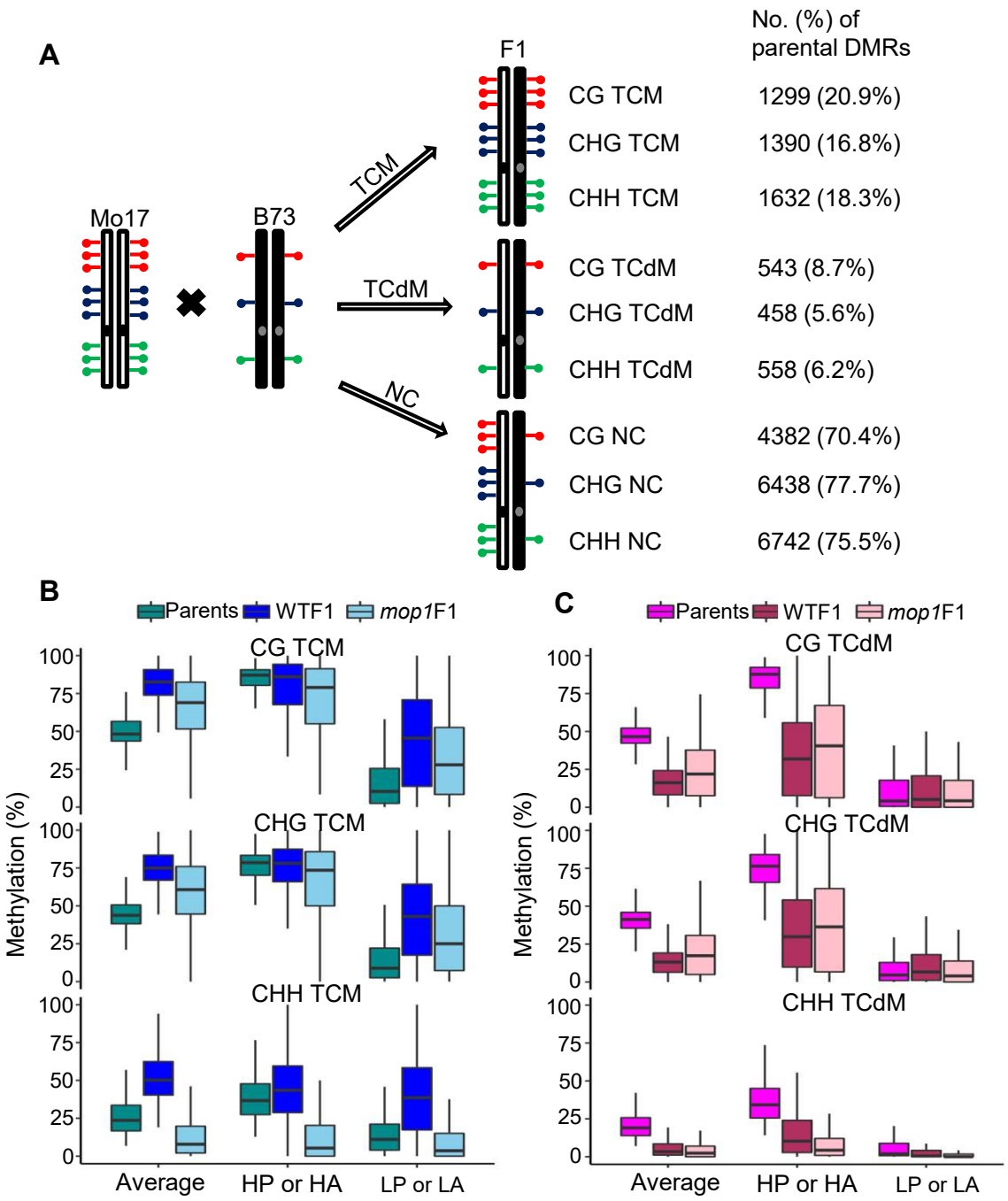

Figure 3. The levels of CHH methylation of both high- and low-parent alleles are increased at TCM DMRs in the F1 hybrids.
(*A*) Identification of TCM, TCdM, and unchanged (NC) DMRs between WTF1 and parents. (*B*) Comparisons of CG, CHG and CHH methylation at TCM DMRs in parents, WTF1 and *mop1*F1. (*C*) Comparisons of CG, CHG and CHH methylation at TCdM DMRs in parents, WTF1 and *mop1*F1. HP, high parent (parent with higher methylation). HA, high-parent allele in F1. LP, low parent (parent with lower methylation). LA, low-parent allele in F1. Average means the average between the two parents, or between the two alleles in WTF1 and *mop1*F1. DMRs, differentially methylated regions. TCM, *trans*-chromosomal methylation. TCdM, *trans*-chromosomal demethylation.

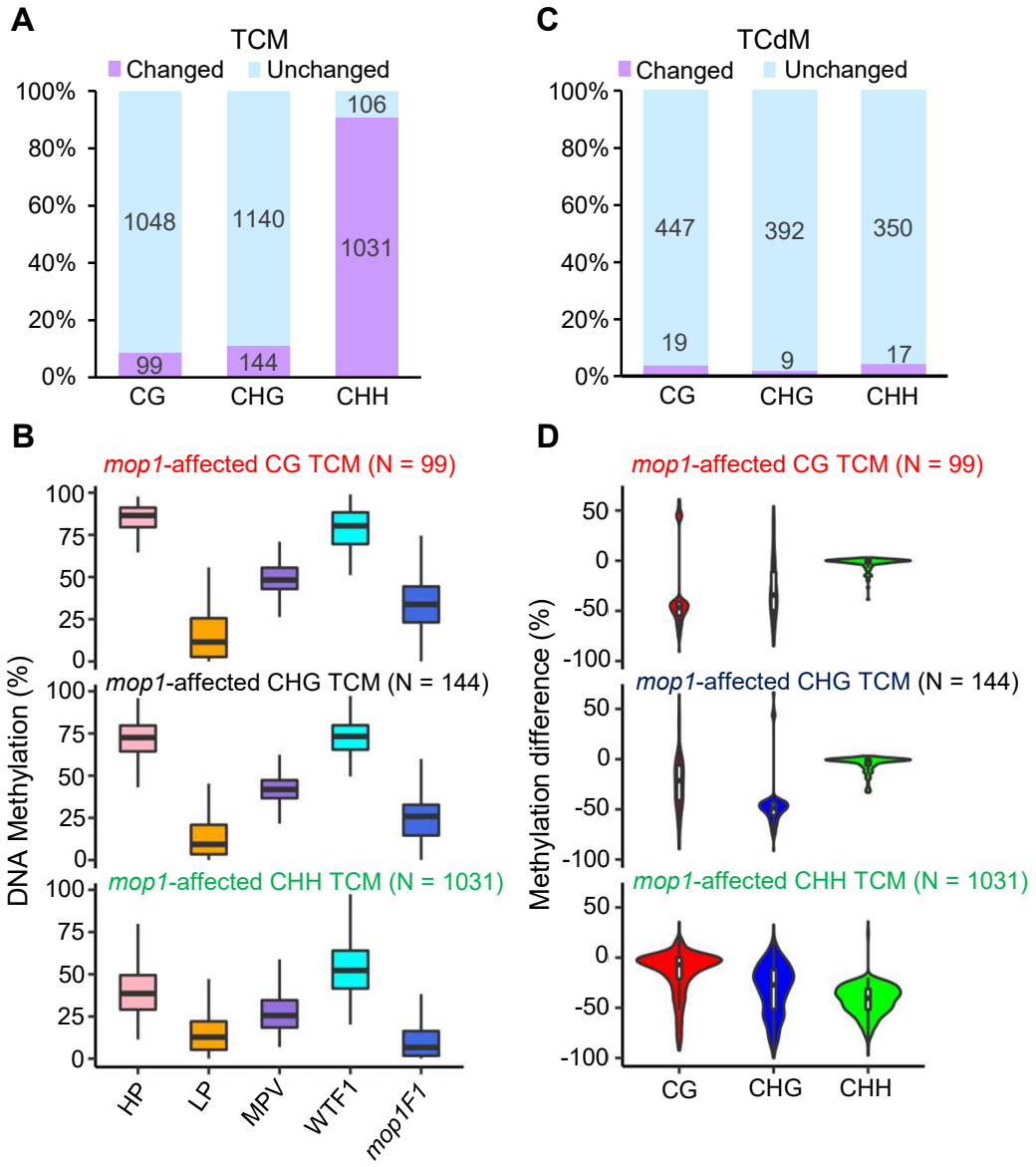

Figure 4. The *mop*1 mutation primarily removes the methylation of CHH TCM DMRs.
(*A*) Number of CG, CHG and CHH TCM DMRs affected by the *mop1* mutation. (*B*) Comparison of methylation levels at the *mop1*-affected CG, CHG, and CHH TCM DMRs. (*C*) Number of CG, CHG and CHH TCdM DMRs affected by the *mop1* mutation. (*D*) Examination of the methylation changes in the other two cytosine contexts at the *mop1*-affected CG, CHG, and CHH TCM DMRs. The top panel shows the methylation changes in CHG and CHH sequence contexts at the 99 *mop1*-affected CG TCM DMRs. The middle panel shows the methylation changes in CG and CHH sequence contexts at the 144 *mop1*-affected CHG TCM DMRs. The bottom panel shows the methylation changes in CG and CHG sequence contexts at the 1031 *mop1*-affected CHH TCM DMRs. HP, high parent (parent with higher methylation). LP, low parent (parent with lower methylation). MPV, the middle parent value. DMRs, differentially methylated regions. TCM, *trans*-chromosomal methylation. TCdM, *trans*-chromosomal demethylation.

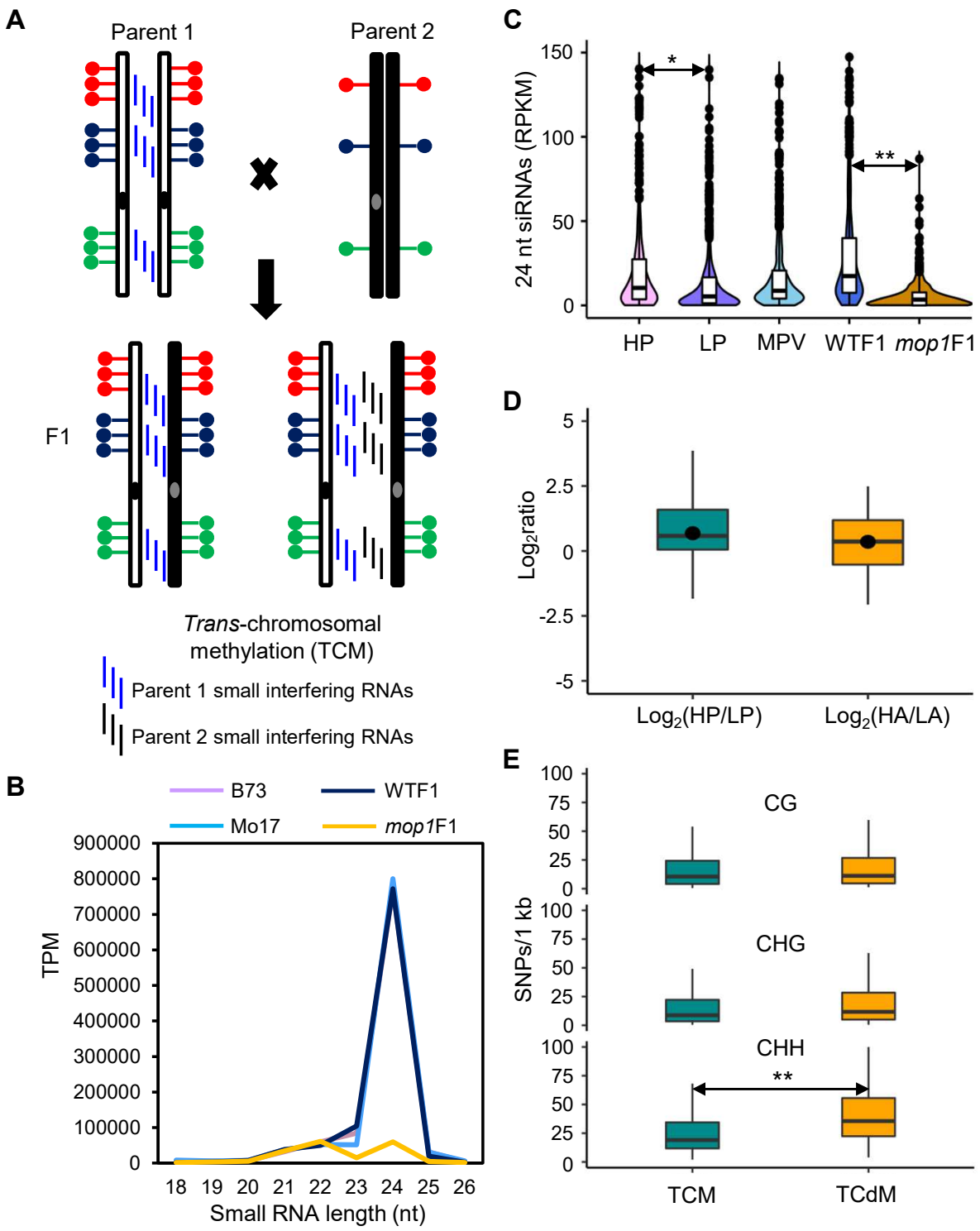

Figure 5. Small RNAs produced from one parent are sufficient to trigger new methylation of the other allele in hybrids.
(*A*) Two hypothetical models of small RNA biogenesis in F1 at CHH TCM. (*B*) Expression values of small RNAs in parents, WTF1 and *mop1*F1. TPM, transcripts per million uniquely mapped reads. The small RNA values were adjusted to total abundance of all mature microRNAs following the previous research (Nobuta et al., 2008). (*C*) The abundance of 24 nt small interfering RNA (siRNAs) at the *mop1*-affected CHH TCM DMRs. HP, high parent (parent with higher methylation). LP, low parent (parent with lower methylation). MPV, the middle parent value. RPKM, 24 nt siRNA reads per kilobase (DMR length) per million uniquely mapped reads. (*D*) Ratios of 24 nt siRNAs of high parent to low parent, and of high-parent allele to low-parent allele at the *mop1*-affected CHH TCM DMRs. (*E*) Number of single nucleotides polymorphisms (SNPs) between TCM and TCdM. **, $P < 0.01$, *, $P < 0.05$, Student's *t* test. DMRs, differentially methylated regions. TCM, *trans*-chromosomal methylation. TCdM, *trans*-chromosomal demethylation.

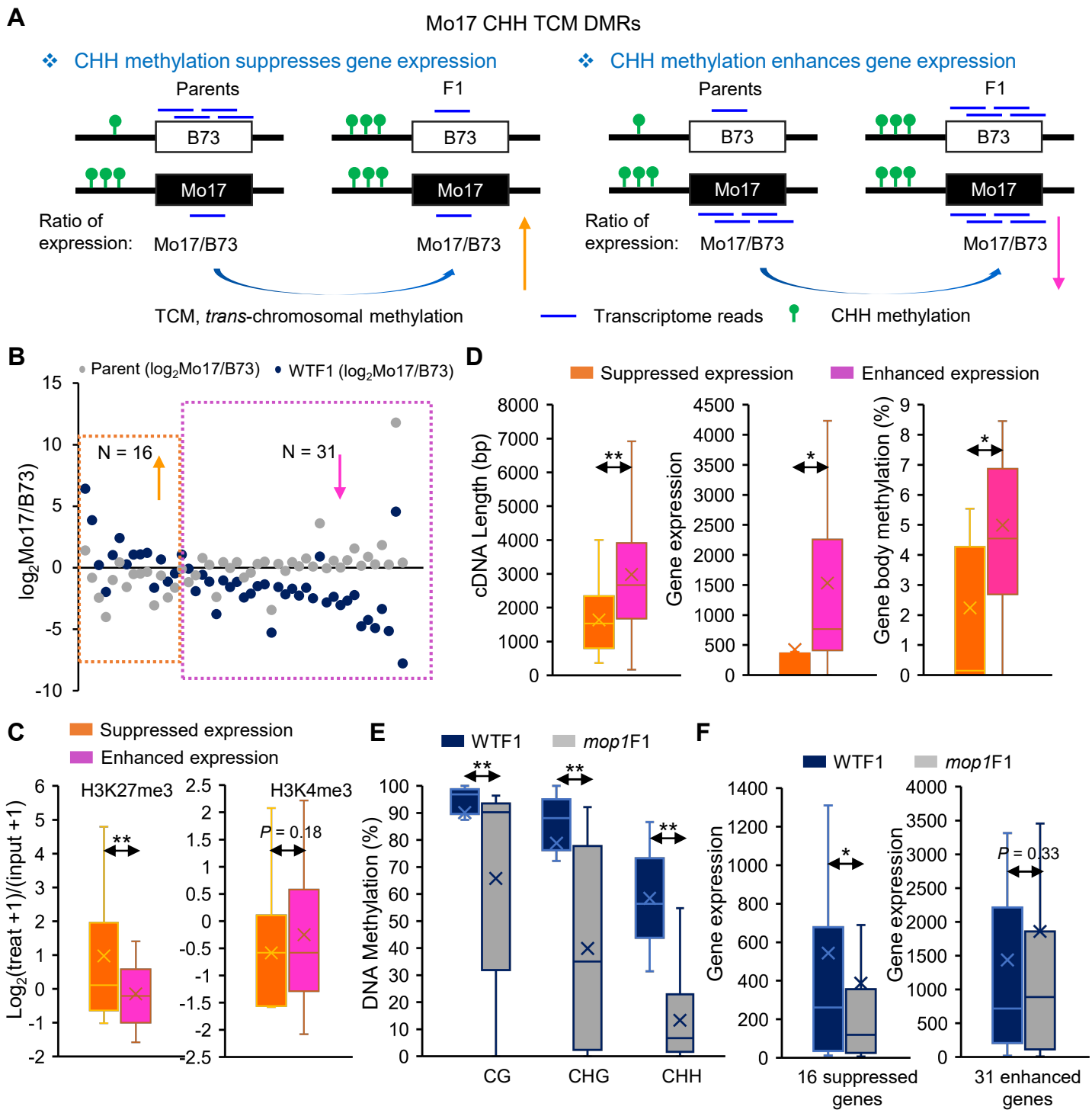

Figure 6. CHH methylation is associated with both suppressed and enhanced expression of their flanking genes.
(*A*) Two possible scenarios of the effects of CHH methylation on gene expression. Here only shows the examples of Mo17 CHH TCM DMRs. (*B*) Number of genes identified based on the models in (*A*). The ratios of expression values of Mo17 to B73 between the parents and WTF1 were used to determine the scenarios. (*C*) Histone modification of 16 CHH TCM DMRs that are associated with the suppressed expression of flanking genes and 31 CHH TCM DMRs that are associated with the enhanced expression of flanking genes. **, $P < 0.01$, Student's *t* test. (*D*) Gene properties of the 16 suppressed and 31 enhanced genes. **, $P < 0.01$, *, $P < 0.05$, Student's *t* test. (*E*) Methylation changes in *mop1* mutants at the 31 CHH TCM DMRs that are associated with the enhanced expression of flanking genes. **, $P < 0.01$, Student's paired *t* test. (*F*) Gene expression changes of the 16 suppressed and 31 enhanced genes in *mop1* mutants. *, $P < 0.01$, Student's paired *t* test. DMRs, differentially methylated regions. TCM, *trans*-chromosomal methylation.

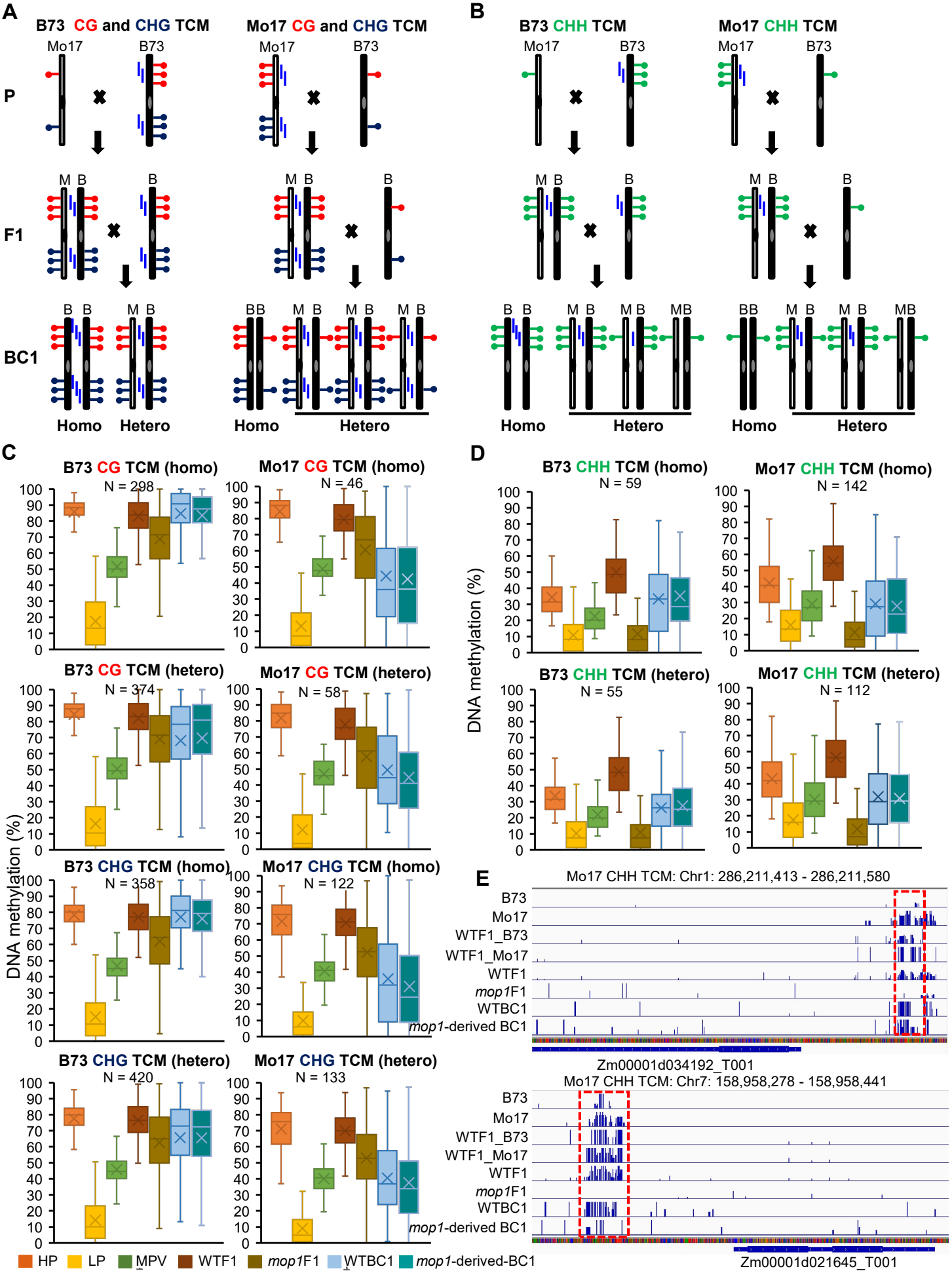

Figure 7. Newly triggered methylation at TCM and demethylation at TCdM DMRs in F1 plants can be maintained in the next generation. (*A*) Hypothetical models assuming maintenance of CG and CHG TCM DMRs. (*B*) Hypothetical models assuming maintenance of CHH TCM DMRs. (*C*) Methylation changes of CG and CHG TCM DMRs. (*D*) Methylation changes of CHH TCM DMRs. (*E*) Distribution and methylation levels of two examples of Mo17 CHH TCM DMRs. DMRs, differentially methylated regions. TCM, *trans*-chromosomal methylation. Homo, homozygous. Hetero, heterozygous.

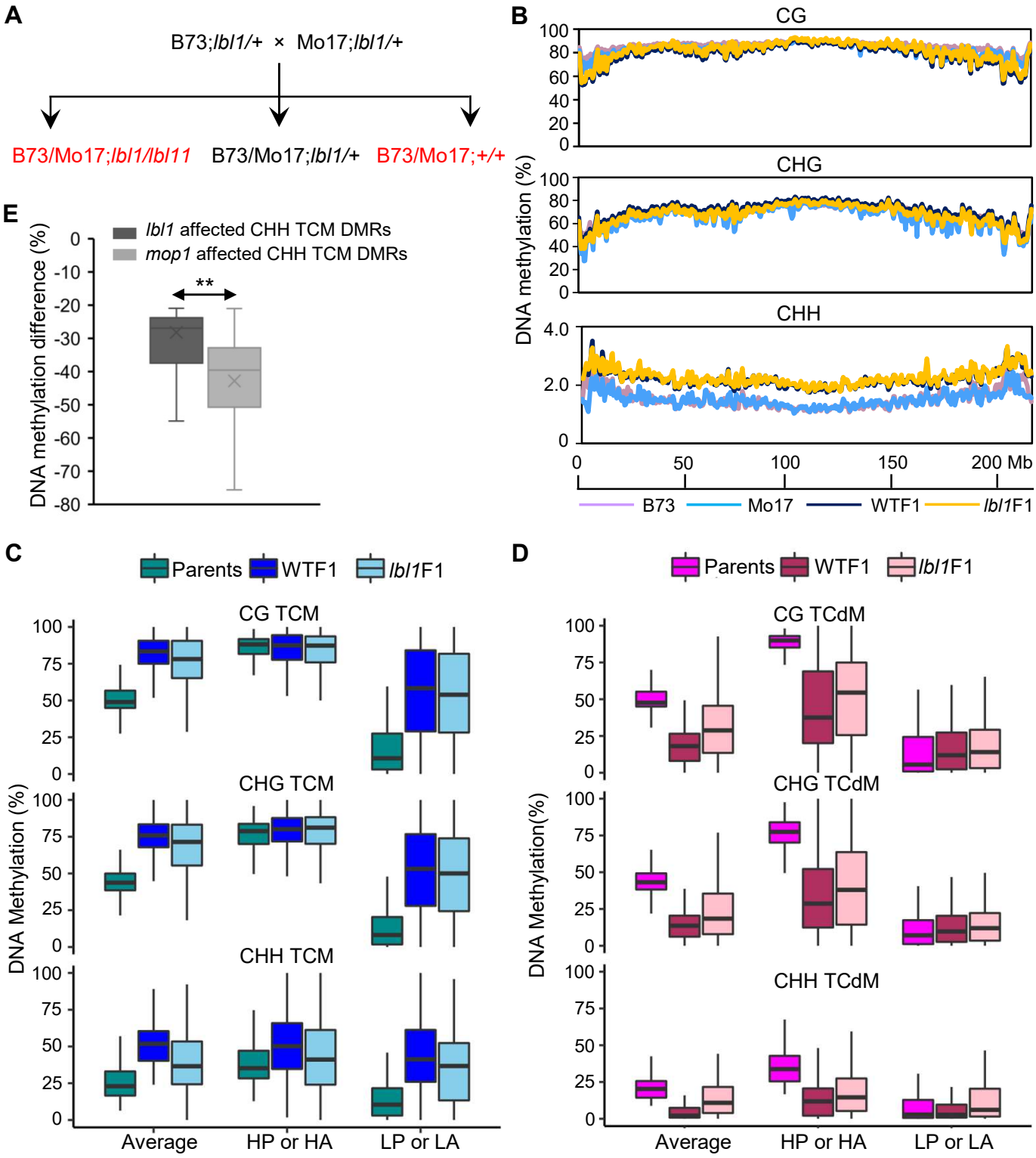

Figure 8. The *lbl1* mutation has less effects on DNA methylation.
(*A*) Genetic strategy to obtain the wild type F1 (WTF1) and *lbl1* mutant F1 (*lbl1*F1). (*B*) The distribution of CG, CHG, and CHH methylation on chromosome 5. Methylation levels were measured in 1 Mb windows with 500 kb shift. (*C*) Comparisons of CG, CHG and CHH methylation at TCM DMRs in parents, WTF1 and *lbl1*F1. (*D*) Comparisons of CG, CHG and CHH methylation at TCdM DMRs in parents, WTF1 and *lbl1*F1. (E) CHH TCM DMRs affected by both *mop*1 and *lbl1* mutations. HP, high parent (parent with higher methylation). HA, high-parent allele in F1. LP, low parent (parent with lower methylation). LA, low-parent allele in F1. Average means the average between the two parents, or between the two alleles in WTF1 and *lbl1*F1. DMRs, differentially methylated regions. TCM, *trans*-chromosomal methylation. TCdM, *trans*-chromosomal demethylation.